Inorganic Chemistry
Cite This: Inorg. Chem. 2019, 58, 13299−13313
Article
pubs.acs.org/IC

Synthesis, Structural Characterization, and Coordination Chemistry of (Trineopentylphosphine)palladium(aryl)bromide Dimer Complexes ([(Np$_3$P)Pd(Ar)Br]$_2$)

Huaiyuan Hu, Monica Vasiliu, Trent H. Stein, Fengrui Qu, Deidra L. Gerlach, David A. Dixon,* and Kevin H. Shaughnessy*

Department of Chemistry and Biochemistry, The University of Alabama, Box 870336, Tuscaloosa, Alabama 35487-0336, United States

Supporting Information

ABSTRACT: A series of [(PNp$_3$)Pd(Ar)Br]$_2$ complexes (PNp$_3$ = trineopentylphosphine, Ar = 4-tolyl, 4-*tert*-butylphenyl, 2-tolyl, 4-methoxy-2-methylphenyl, 2-isopropylphenyl, and 2,6-dimethylphenyl) were synthesized and structurally characterized by X-ray crystallography and density functional theory optimized structures. The trineopentylphosphine ligand is able to accommodate coordination of other sterically demanding ligands through changes in its conformation. These conformational changes can be seen in changes in percent buried volume of the PNp$_3$ ligand. The binding equilibria of the [(PNp$_3$)Pd(Ar)Br]$_2$ complexes with pyridine derivatives were determined experimentally and analyzed computationally. The binding equilibria are sensitive to the steric demand of the pyridine ligand and less sensitive to the steric demand of the aryl ligand on palladium. In contrast to previous studies, the binding equilibria do not correlate with pyridine basicity. The binding equilibria results are relevant to fundamental ligand coordination steps in cross-coupling reactions, such as Buchwald−Hartwig aminations.

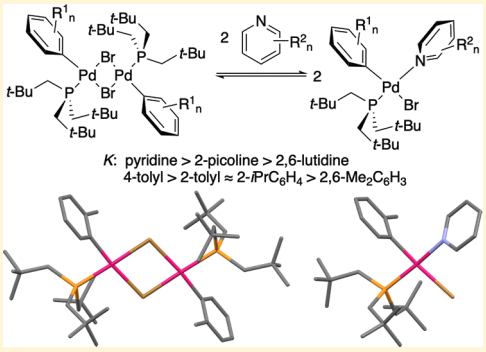

INTRODUCTION

Oxidative addition of aryl halides to palladium(0) to afford L$_n$Pd(Ar)X complexes is a fundamental step in all palladium-catalyzed cross-coupling reactions. With less reactive substrates, such as aryl chlorides and sulfonates, this step is often rate limiting. Significant effort has been devoted to the development of ligands affording highly active catalysts capable of promoting cross-coupling of challenging substrates. Sterically demanding, electron-rich ligands, such as dialkylbiarylphosphines,[1] trialkylphosphines,[2] bis(dialkylphosphine) ligands,[3] and *N*-heterocyclic carbenes,[4] are particularly useful in promoting these reactions. The strong electron-donating ability of these ligands promotes the oxidative addition step. Sterically demanding ligands promote transient low-coordinate LPd(0) species that are highly reactive toward oxidative addition. In addition, sterically demanding ligands can promote reductive elimination in cases where that is the rate limiting step.

Commonly used sterically demanding, electron-rich ligands, such as P(*t*-Bu)$_3$, Buchwald-type ligands (S-Phos, RuPhos, X-Phos), and NHCs (IPr, IMes), have relatively rigid structures with fixed steric demand. Sterically demanding ligands can limit the ability of complexes to couple sterically demanding substrates. For example, commonly used catalyst systems based on tri-*tert*-butylphosphine (P(*t*-Bu)$_3$) or S-phos give low yields in the coupling of 2,6-disubstituted anilines and 2,6-disubstituted aryl bromides.[5] Whereas simple palladium/phosphine precatalysts are often ineffective for coupling of hindered aryl halides and amines, NHC-palladium precatalysts,[6] phosphatrane/palladium complexes,[7] and diketiminate complexes[8] are effective for sterically demanding substrates.

Our group has explored neopentylphosphines in palladium-catalyzed cross-coupling reactions. Catalysts derived from di(*tert*-butyl)neopentylphosphines ((*t*-Bu)$_2$PNp) are effective for cross-coupling of aryl bromides and chlorides with a variety of nucleophilic coupling partners.[9] The (*t*-Bu)$_2$PNp ligand has limited flexibility, and catalysts derived from it generally give low conversion with sterically demanding substrates. In contrast, trineopentylphosphine (PNp$_3$) is able to tolerate sterically demanding substrates to afford high yields in couplings with amines, arylboronic acids, and ketones.[9d,10] We have hypothesized that the conformational flexibility of PNp$_3$ shown in solid state structures allows it to accommodate sterically demanding substrates. A kinetic study of the oxidative addition of aryl bromides to Pd(PNp$_3$)$_2$ showed that the reaction rate is unaffected by the steric effects of the aryl bromide.[11]

To gain a better understanding of the ability of PNp$_3$ to facilitate coupling of sterically demanding substrates, we sought

Received: July 19, 2019
Published: September 25, 2019

DOI: 10.1021/acs.inorgchem.9b02164
Inorg. Chem. 2019, 58, 13299−13313

to prepare and characterize a series of $[(PNp_3)Pd(Ar)Br]_2$ complexes where the aryl group would have zero, one, or two *ortho* substituents. Examples of isolated and structurally characterized palladium complexes with 2,6-disubstituted aryl substituents are rare in the literature.[12] Successful isolation of products of oxidative addition of 2,6-disubstituted aryl halides to triphenylphosphine[13] and tri(*ortho*-tolyl)phosphine[14] palladium complexes have been reported, but no examples had been structurally characterized prior to our work in this area.

We have previously reported the synthesis of 2-tolyl and 2,6-dimethylphenyl palladium complexes with PNp_3 as the supporting ligand.[10,11] Herein, we report additional examples of $[(Np_3P)Pd(Ar)Br]_2$ complexes and provide a more detailed structural and computational analysis of these complexes. We also report an experimental and computational study of the dimer cleavage reaction of $[(PNp_3)Pd(Ar)Br]_2$ with pyridine derivatives having varied steric demand to afford $(PNp_3)Pd(Ar)(pyridine)Br$ complexes as well as synthesis of $(PNp_3)Pd(Ar)$amine complexes relevant to Buchwald–Hartwig amination reactions.

RESULTS AND DISCUSSION

Synthesis of Aryl Palladium Dimers and Solid State Geometry. Halide bridged aryl palladium complexes of the formula $[(PNp_3)Pd(Ar)Br]_2$ (Ar = 4-tolyl (**3a**), 4-*tert*-butylphenyl (**3b**), 2-tolyl (**3c**), 4-methoxy-2-methylphenyl (**3d**), and 2-isopropylphenyl (**3e**)) were synthesized from the oxidative addition of the corresponding aryl bromide (**2a–2e**) to $Pd(PNp_3)_2$ (**1**) in toluene at 70 °C (eq 1). Complex **3f**

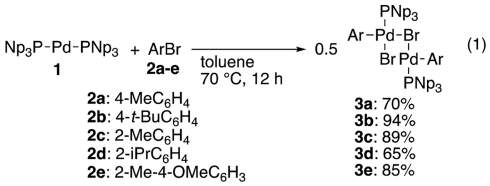

cannot be prepared by oxidative addition to **1** and was prepared by the reaction of $(COD)Pd(CH_2TMS)_2$ with **2f** and PNp_3.[11] The syntheses of **3b**,[10] **3c**,[10] and **3f**[11] have been previously reported by us. Newly reported complexes **3a**, **3d**, and **3e** were obtained in 65–80% isolated yield as air-stable solids. In solution, the complexes exist as equilibrium mixtures of stereoisomers. For example, complex **3a** gives two resonances in the ^{31}P NMR spectrum in a 7.7:1 ratio in C_6D_6 due to *trans* and *cis* dimeric structures. Complexes **3d** and **3e** give four resonances due to *trans* and *cis* dimeric structures and *anti* and *syn* relationships between the *ortho* substituents.[10] Crystal structures of complexes **3b** (Supporting

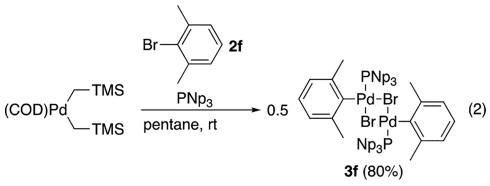

Information, Figure S24),[10] **3c** (Figure S25),[10] and **3f** (Figure S26)[11] have been previously reported by us. X-ray quality crystals of **3a** and **3e** were grown by slow evaporation in a mixture of methylene chloride and heptane at 22 °C. Complex **3a** (Figure 1) crystallized with two molecules in the asymmetric unit. One molecule (Figure 1) has a planar halide

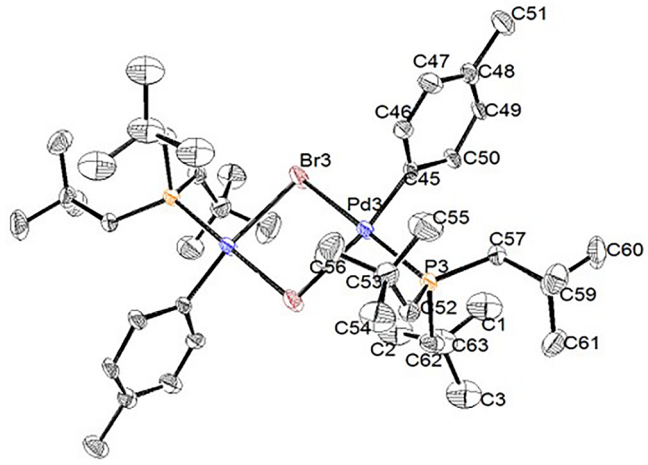

Figure 1. Thermal ellipsoid plot (50% probability) of the planar molecular structure of **3a**. Hydrogen atoms and disorder are omitted for clarity.

bridged dimer structure with inversion symmetry relating the two $(PNp_3)Pd(4\text{-}C_6H_4Me)Br$ units similar to that seen in complexes **3b–3f**. The other molecule (Figure S20, Supporting Information) in the asymmetric unit has a butterfly geometry in which the angle between the two palladium square planes is 148.1°. Palladium dimer **3e** crystallized as a symmetric planar halide-bridged dimer with similar structural features to the previously reported **3b**, **3c**, and **3f** (Figure 2).

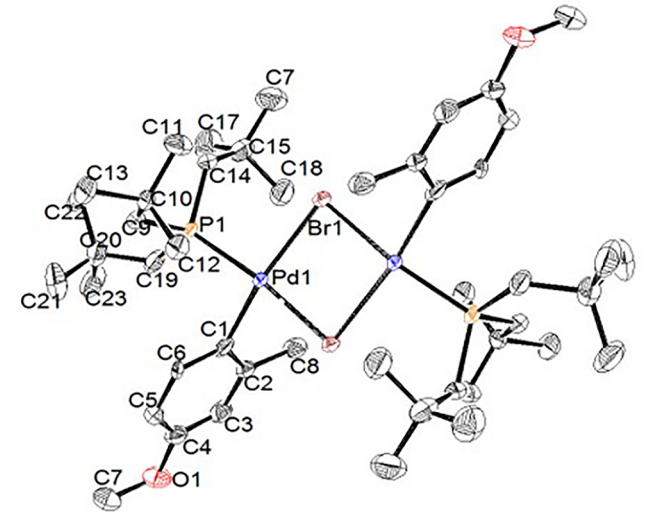

Figure 2. Thermal ellipsoid plot (50% probability) of the molecular structure of **3e**. Hydrogen atoms are omitted for clarity.

Structural Comparison of Solid State Structures of $[(PNp_3)Pd(Ar)Br]_2$. Comparison of the palladium–ligand bond lengths shows how increasing steric demand of the aryl ligand affects bonding to the palladium center (Table 1). The Pd–C bond lengths for structures **3a–3f** show no statistically significant difference as *ortho* substituents are added. The increased steric demand of the aryl ligand does have a small but statistically significant effect on the Pd–P bond distance, however. The Pd–P bond distances are 2.248(1) and 2.245(1) Å for **3a** and **3b**, respectively, whereas the *ortho*-substituted compounds (**3c**, **3e**, and **3f**) have longer Pd–P bond lengths

DOI: 10.1021/acs.inorgchem.9b02164
Inorg. Chem. 2019, 58, 13299–13313

Table 1. Experimental and Calculated B3LYP/DZVP2(H,C,N,P)/DZVP(Br)/aug-cc-pVDZ-PP(Pd) Selected Bond Lengths and Angles of $[(Np_3P)Pd(Ar)Br]_2$ Complexes

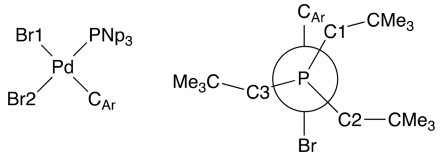

property	3a[a]	3a calcd	3b	3b calcd	3c	3c calcd	3e	3e calcd	3f	3f calcd	4[b]
Pd–Br1 (Å)	2.597(5)	2.67	2.5978(7)	2.67	2.573(2)	2.66	2.582(1)	2.66	2.5814(4)	2.66	—[c]
Pd–Br2 (Å)	2.561(7)	2.58	2.4992(7)	2.58	2.506(2)	2.58	2.529(1)	2.58	2.5060(3)	2.57	—[c]
Pd–P (Å)	2.248(1)	2.31	2.245(1)	2.31	2.266(3)	2.33	2.283(2)	2.32	2.2710(3)	2.34	2.219(2)
Pd–C_{Ar} (Å)	1.94(7)	2.01	2.003(5)	2.01	2.00(2)	2.01	2.03(1)	2.02	2.009(1)	2.02	2.002(6)
Br1–Pd–P (deg)	92.5(2)	93.9	92.50(4)	94.0	97.51(9)	97.3	98.45(6)	97.5	97.49(1)	97.5	91.59(6)[c]
C_{Ar}–Pd–P (deg)	94(2)	91.8	91.4(1)	91.9	88.1(4)	89.8	88.5(2)	89.9	91.31(4)	92.0	89.3(2)
Br2–Pd–C_{Ar} (deg)	88(2)	88.6	89.8(1)	88.5	87.6(4)	88.1	87.4(2)	88.0	85.52(4)	86.4	92.3(2)[c]
Br1–Pd–Br2 (deg)	87.2(2)	85.8	86.56(2)	85.6	86.87(6)	84.7	86.38(3)	84.5	85.68(1)	84.2	86.74(6)[c]
P–Pd–Br2 (deg)	171.1(2)	179.4	177.27(4)	178.6	172.9(1)	176.8	170.64(7)	176.8	176.44(1)	176.7	178.13(6)[c]
C_{Ar}–Pd–Br1 (deg)	171(2)	174.2	174.5(1)	173.9	174.4(4)	172.2	171.7(2)	172.1	171.19(4)	170.5	179.0(2)[c]
Pd–P–C1–C (deg)	177.0(3)	174.1	179.9(4)	174.0	152(1)	154.8	151.0(7)	154.4	163.9(1)	163.0	174.1(4)
Pd–P–C2–C (deg)	57.0(4)	56.5	50.4(4)	46.6	72(1)	69.4	71.3(8)	70.4	60.9(1)	57.6	64.6(6)
Pd–P–C3–C (deg)	49.5(4)	46.0	55.8(4)	56.2	52(1)	49.4	46.5(8)	49.7	49.9(1)	49.6	61.2(5)
C_{Ar}–Pd–P–C1 (deg)	5(2)	3.2	6.9(2)	3.1	30.2(7)	32.7	24.5(4)	32.1	14.86(6)	13.3	7.2(3)
C1–P–C2 (deg)	107.9(2)	108.1	108.9(2)	108.4	108.4(6)	107.4	108.5(4)	107.8	108.55(6)	107.4	104.0(3)
C2–P–C3 (deg)	99.2(2)	99.2	100.6(2)	99.1	104.4(6)	103.8	103.1(4)	103.9	101.66(6)	102.1	104.9(3)
C3–P–C1 (deg)	108.7(2)	108.2	108.3(2)	107.8	104.8(6)	104.7	105.4(4)	104.5	101.63(6)	101.8	105.0(3)
P–C1–C (deg)	127.1(3)	128.1	127.5(4)	128.2	129(1)	127.8	126.9(7)	127.9	128.7(1)	128.6	116.2(5)
P–C2–C (deg)	122.7(4)	123.9	121.9(4)	122.9	122(1)	123.8	123.3(7)	123.8	125.57(9)	125.5	112.0(5)
P–C3–C (deg)	122.8(3)	122.7	121.9(4)	123.7	124(1)	125.0	125.4(6)	125.0	126.5(1)	127.0	112.9(5)
$\%V_b$[d]	36.3	34.7	37.6	34.6	34.7	32.5	34.3	32.6	32.3	30.9	28.2

[a]Measurements taken from planar dimeric structure (Figure 1). [b]$[(Et_3P)Pd(4\text{-tolyl})Cl]_2$.[15] [c]Chloride in place of bromide. [d]$\%V_b$ calculated using the SambVca 2.0 Web application.[16]

DOI: 10.1021/acs.inorgchem.9b02164
Inorg. Chem. 2019, 58, 13299−13313

(2.266(3)−2.282(2) Å). The Pd−Br bonds were similar for all of the complexes. The Pd−Br1 bond is longer than Pd−Br2 for each of the complexes due to the stronger *trans* effect of the aryl substituent compared to the phosphine. Comparison of the PNp_3 complexes with $[(Et_3P)Pd(4\text{-tolyl})Cl]_2$ (**4**) shows a similar trend. The Pd−C bond for **4** is the same as those seen with complexes **3a**−**3f**. The smaller PEt_3 ligand has a shorter Pd−P bond length (2.219 Å) compared to **3a** (2.248 Å), indicating the increased steric effect of the neopentyl substituents compared to ethyl.

The bond angles around the palladium center show more variation as a result of an increased steric demand due to the aryl ligand (Table 1). For complexes **3a** and **3b** with *para*-substituted aryl ligands, the angles around palladium are all close to 90° as expected in a square planar geometry. The values for **3b** are similar to that of the PEt_3 complex (**4**). For the complexes with *ortho*-substituted aryl ligands, the square planar geometry is distorted to accommodate the bulky PNp_3 and aryl ligands. In each case (**3c**, **3e**, **3f**), the Br1−Pd−P angle is significantly increased (97.5−98.5°). In complexes **3c** and **3e**, the C_{Ar}−Pd−P angle decreases by approximately 2° as does the Br2−Pd−C_{Ar} angle. The 2,6-dimethylphenyl complex (**3f**) has a larger C_{Ar}−Pd−P angle than **3c** or **3e** due to increased steric repulsion, which results in smaller Br2−Pd−C_{Ar} and Br1−Pd−Br2 angles (85.52, 86.68°). The overall effect is that *ortho* substituents cause the PNp_3 and aryl ligands to move away from Br1 and toward Br2 in the square plane.

Compared to commonly used sterically demanding trialkylphosphines, such as tri-(*tert*-butyl)phosphine, trineopentylphosphine has a higher degree of conformational flexibility. This flexibility can be seen in the conformation changes of the PNp_3 coordinated to metal centers with different coordination numbers. In the two-coordinate Pd-$(PNp_3)_2$ complex, the neopentyl groups adopts a C_3 symmetrical conformation in which the substituents are oriented toward the metal center with small Pd−P−C−C dihedral angles (34°).[10] In contrast, when PNp_3 is coordinated to four-coordinate metal centers, as in the case of complexes **3a**−**3f**, the neopentyl groups adopt a conformation in which one neopentyl group is approximately *anti* to the Pd−P bond. The other two neopentyl substituents adopt pseudogauche conformations relative to the Pd−P bond and are positioned above and below the Pd_2Br_2 plane. The trineopentylphosphine conformation is similar to that seen in $[(Et_3P)Pd(4\text{-tolyl})Cl]_2$ (**4**).[15]

The conformation of the PNp_3 ligand in the $[(PNp_3)$-$PdArBr]_2$ complexes is affected by the presence of *ortho*-substituents on the aryl ligand (Figure 3). When the aryl group has no *ortho* substituents (**3a** and **3b**), the PNp_3 ligand adopts a conformation with pseudomirror plane symmetry in which one neopentyl substituent (C1) is nearly eclipsed with the Pd−C_{Ar} bond (C1−P−Pd−C_{Ar} = 4.93 (**3a**), 6.94 (**3b**); Table 1) and has an *anti* relationship to the Pd−P bond (Pd−P−C1−C 177−180°). The other two neopentyl groups are oriented above and below the palladium square plane with roughly gauche relationships to the Pd−P bond (Pd−P−C−C = 50−56°). The *anti*-neopentyl substituent (C1) repels the other two neopentyl substituents, resulting in large C1−P−C2 and C1−P−C3 angles (107.9−108.8°). As a result, the C2−P−C3 angle is much smaller (99.2° (**3a**), 100.6° (**3b**)). In contrast, the C−P−C angles of the PEt_3 ligand in **4** are all similar (104−105°). The P−C−C bond angle for all three neopentyl groups are significantly expanded (122−127°) with the *anti*-neopentyl group having the largest P−C−C bond angle. These values are considerable larger than the P−C−C angles for the ethyl substituents in **4** (112−116°).

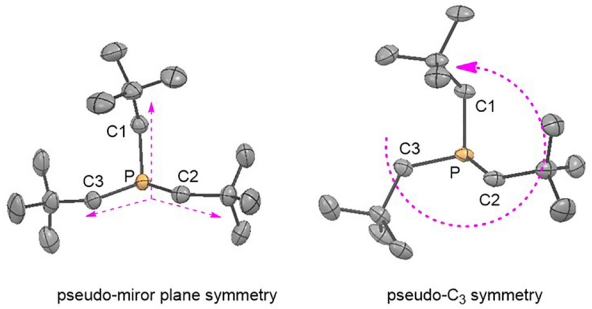

Figure 3. Trineopentyl conformations observed for **3a**−**3f**. Pseudomirror plane (**3a**, **3b**) and pseudo-C_3 (propeller type, **3c**, **3e**, and **3f**).

When *ortho* substituents are present on the aryl ligand, the PNp_3 ligand adopts a pseudo-C_3 propeller-type geometry (Figure 3). In the case of **3c** with a 2-tolyl ligand, the phosphine rotates to move the C1 neopentyl substituent toward the methyl substituent on the 2-tolyl ligand (C1−P−Pd−C_{Ar} = 30.2°). The Pd−P−C1−C dihedral angle decreases to 152.48°, consistent with the neopentyl group rotating away from the ortho methyl and toward the face of the arene. The C2 neopentyl has a larger Pd−P−C2−C dihedral angle (72°) to accommodate the C1 neopentyl group. The dihedral angle for the C3 neopentyl group is similar to that in **3a** and **3b**. The C1−P−C2 angle (108.4°) for **3c** is still larger than the C2−P−C3 (104.4°) and C3−P−C1 (104.8°) angles, but the difference is smaller than for **3a** and **3b**. The P−C1−C angle is again the largest (129°) in **3c**, but the P−C3−C angle is also expanded (124°) in response to the strain on this substituent. Complex **3e** gives similar structural parameters.

The PNp_3 ligand in the 2,6-dimethylphenyl complex (**3f**) adopts a similar pseudo-C_3 conformation to that seen in the complexes with mono-*ortho*-substituted aryl ligands (**3c** and **3e**). The dihedral angle between the aryl ligand and the C1 neopentyl group (14.86°) is smaller than in **3c** but larger than **3a** or **3b**. Like **3c**, the C1 neopentyl group in **3f** is not completely *anti* (Pd−P−C1−C = 163.9°) to the Pd−P bond. The dihedral angle for the C2 neopentyl substituent (60.9°) is larger than for the C3 neopentyl group, although not as large as observed for **3c** or **3e**. To accommodate the larger aryl ligand, the P−C1−C3 and P−C2−C3 angles are smaller (101.6°) in **3f** than in **3c** (104°). As a result, the PNp_3 ligand is more pyramidalized than in the other complexes (Σ_{C-P-C}: **3a** = 315.9°, **3b** = 317.7°, **3c** = 317.6°, **3e**, 316.9°, **3f** = 311.84°). The two neopentyl substituents projected toward the palladium center have larger P−C2−C and P−C3−C angles than in **3a**−**3e** to accommodate the additional strain.

The most notable evidence of the steric strain experienced by the PNp_3 ligand is the expanded P−C−C bond angles in the neopentyl substituents, particularly the *anti*-oriented neopentyl (P−C1−C). Complex **3f** has the largest P−C1−C value of 128.7°. The bond angles at the neopentyl methylene carbons are among the largest reported in the literature for a tetravalent carbon. Examples of molecules with comparable bond angles at a methylene carbon include di(*tert*-butyl)-methane (121−128°)[17] and $CH_2(SF_5)_2$ (126°).[18]

These conformational changes have a noticeable effect on the steric demand of the PNp_3 ligand as measured by the

DOI: 10.1021/acs.inorgchem.9b02164
Inorg. Chem. 2019, 58, 13299−13313

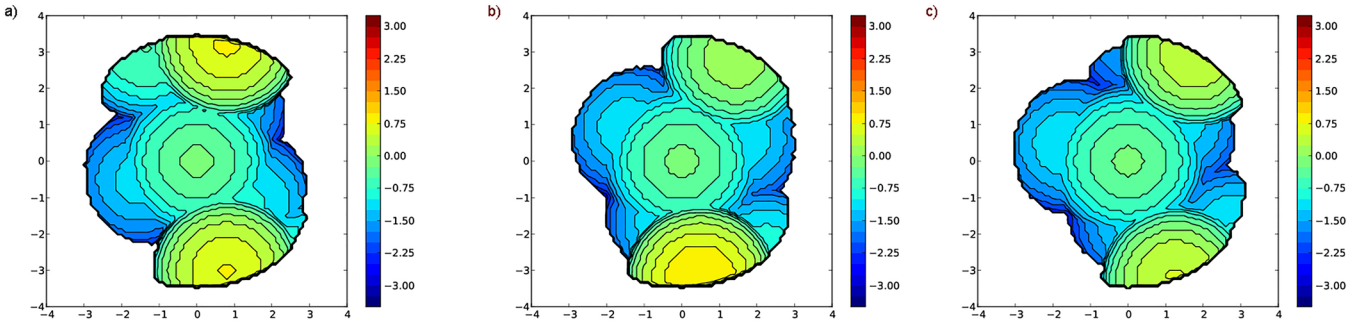

Figure 4. Steric contour maps obtained from the SambVca 2.0 Web Application.[16] The metal is at the center of a sphere with a radius of 3.5 Å. Positive values (yellow-red) reflect substituents projecting into the lower hemisphere past the metal. (a) **3a**, (b) **3c**, (c) **3f**.

percent buried volume (%V_b). The %V_b parameter calculated using the SambVca 2.0 Web Application[16] was determined from the solid state structures of **3a**, **3b**, **3c**, **3e**, and **3f**, as well as previously reported complex **4** (Table 1). In Pd-$(PNp_3)_2$Pd,[10] in which the neopentyl substituents all point toward the metal center, the %V_b is 42.3%. This value decreases in complexes **3a** (36.3%) and **3b** (37.4%) as the PNp_3 conformation changes. The addition of *ortho*-methyl substituents in **3c** (34.7%), **3e** (34.3%), and **3f** (32.3%) results in a further decrease in the buried volume as the ligand is repelled away from the aryl ligands.

The decrease in buried volume for the ligands appears to result from a combination of structural changes. As *ortho* substituents are added to the aryl ligand, the sum of the P−C2−C and P−C3−C angles increases (**3a**, 245.5°; **3c**, 246.5°; **3f**, 252.1°). In the case of **3f**, there is also a significant increase in the pyramidalization at phosphorus, although **3c** and **3e** have similar Σ_{C-P-C} angles to **3a** and **3b**. These structural changes have the effect of moving the $-C(CH_3)_3$ group away from the metal center, particularly for **3f**. Steric contour maps for complexes **3a**, **3c**, and **3f** show that the neopentyl methyl groups closest to the metal center, for example, C2 and C56 in **3a**, move away from the metal center and have a decreased steric impact as the steric demand of the aryl ligand increases (Figure 4).

Bromide Bridge Cleavage by Pyridines. Cleavage of the halide-bridged palladium aryl complexes by nucleophilic ligands is anticipated to be a key step in cross-coupling reactions with sterically demanding monodentate ligands. For example, in the Buchwald−Hartwig amination, the amine nucleophile cleaves the dimer to give an amine adduct that is deprotonated, leading to the coupled product.[14] The mechanism of the cleavage of square planar, halide bridged palladium and platinum complexes with amine[19] and alkene[20] ligands has been studied. Kinetic studies are consistent with an associative mechanism with a competitive solvent-mediated pathway. As expected for an associative process, steric demand of the incoming ligand decreases the rate of the dimer cleavage reaction.[19c] In contrast, binding equilibria are more dependent on the basicity of the incoming ligand. In the cleavage of $[(Pr_3P)PdI_2]_2$ with pyridine derivatives, 2,6-lutidine gave a higher equilibrium constant (2670) than pyridine (596) presumably due to the high basicity of lutidine.[19b] In studying the mechanism of the Pd/PNp_3-catalyzed amination reaction, we found that aniline gave no observable reaction with palladium dimers **3b** and **3c**.[11] We therefore sought to use more strongly coordinating nitrogen ligands to analyze this reaction and the effect of the steric demand of the aryl ligand on ligand binding.

Complexes **3a**, **3c**, **3d**, and **3f** were reacted with pyridine (**5a**), 2-picoline (**6b**), and 2,6-lutidine (**5c**) in CD_2Cl_2 (eq 3).

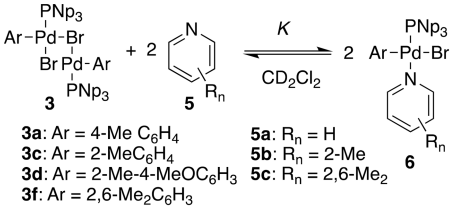

(3)

3a: Ar = 4-Me C_6H_4
3c: Ar = 2-MeC_6H_4
3d: Ar = 2-Me-4-MeOC_6H_3
3f: Ar = 2,6-$Me_2C_6H_3$

5a: R_n = H
5b: R_n = 2-Me
5c: R_n = 2,6-Me_2

6	3	5	6	3	5
6aa	**3a**	**5a**	**6da**	**3d**	**5a**
6ab	**3a**	**5b**	**6db**	**3d**	**5b**
6ac	**3a**	**5c**	**6dc**	**3d**	**5c**
6ca	**3c**	**5a**	**6fa**	**3f**	**5a**
6cb	**3c**	**5b**	**6fb**	**3f**	**5b**
6cc	**3c**	**5c**	**6fc**	**3f**	**5c**

Upon the addition of the pyridine derivative, a new peak was observed by ^{31}P NMR spectroscopy located upfield of the halide-bridged dimer corresponding to the pyridine adduct (**6**). In the majority of cases, incomplete conversion to the pyridine adduct was observed. For each combination, the reactions reached equilibrium by the time the samples could be analyzed (<5 min) and the relative concentrations of **3**, **5**, and **6** did not change over time. In most cases, a single pyridine adduct was observed by ^{31}P NMR spectroscopy. When complex **3a** was reacted with 2-picoline, two new resonances were observed by ^{31}P NMR spectroscopy in a 4:1 ratio. Both peaks were in the region where the other pyridine adducts were observed. We hypothesize that these peaks may indicate the presence of two stereoisomers of **6ab** in solution. For combinations with larger equilibrium constants, it was possible to crystallize the adducts. X-ray quality crystals of **6aa**, **6ca**, **6da**, and **6db** were grown by slow evaporation of methylene chloride solutions containing excess pyridine (Figure 5 and S27−S29). In each case, the pyridine adduct is a monopalladium complex with the pyridine ring coordinated *cis* to the aryl group and *trans* to the phosphine. This geometry places the weakest *trans*-effect ligand (Br) *trans* to the strongest (aryl). This stereochemistry suggests a potential isomerization during the cleavage reaction. In the dimer, the Br *trans* to the aryl ligand has a longer Pd−Br bond and would be expected to be more easily cleaved. The resulting product with pyridine *trans* to the aryl ligand would not be expected to be thermodynamically preferred, however. The observation of two ^{31}P NMR resonances for **6ab** suggests that both stereoisomers may exist in equilibrium in solution.

DOI: 10.1021/acs.inorgchem.9b02164
Inorg. Chem. 2019, 58, 13299−13313

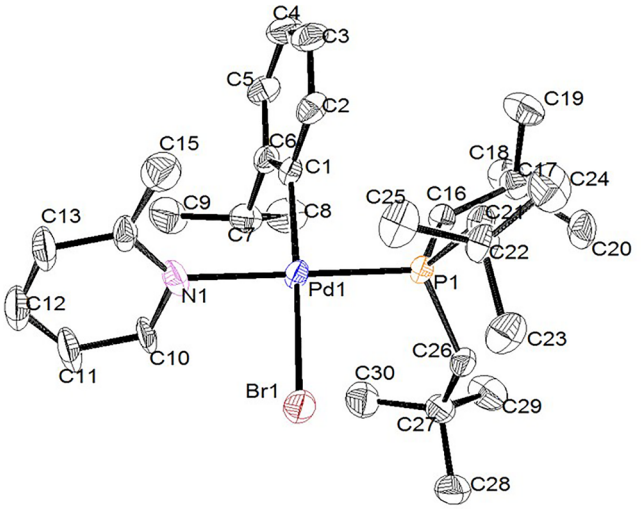

Figure 5. Thermal ellipsoid plot (50% probability) of the molecular structure of **6db**. Hydrogen atoms and disorder are omitted for clarity.

Both the aryl and pyridine ligand are approximately perpendicular to the palladium square plane. The structures of the pyridine complexes are similar to the corresponding halide-bridged dimer (Table S10). In complexes **3** and **6**, the P−Pd−Br angle is the largest angle between the *cis* ligands and becomes larger when the aryl ligand has an *ortho* substituent. The bond angles for the neopentyl ligands in **3a** (Ar = 4-tolyl) and **6aa** (Ar = 4-tolyl, L = pyridine) or in **3c** (Ar = 2-tolyl) and **6ca** (Ar = 2-tolyl, L = 2-picoline) are very similar to each other. This result suggests that the aryl substituent *cis* to PNp_3 plays the largest role in determining the conformation of the phosphine, whereas the *trans* ligand does not have a significant effect on the PNp_3 conformation. A comparison of **6da** and **6db** where the aryl group (2-isopropylphenyl) is the same but the *trans* pyridine group is different (**6da** = pyridine, **6db** = 2-picoline) again shows qualitatively similar structures. The main difference is that the C_{Ar}−Pd−P−C1 dihedral angle for **6da** (17.0°) is significantly smaller than for **6db** (34.12°). The additional rotation of the PNp_3 ligand in **6db** is likely due to repulsion between the *ortho*-methyl group on 2-picoline and the C2 neopentyl group of the phosphine. The limited effect of the pyridine ligands on the PNp_3 ligand can also be seen in the $\%V_b$ values. The values for the pyridine adducts (**6**) are nearly identical to those for the halide dimers (**3**). For example, 4-tolyl complex **3a** and its pyridine adduct (**6aa**) have the same $\%V_b$ value of 36.3%. Notably, the identity of the *ortho* substituent on the aryl ligand (methyl vs isopropyl) does not affect the buried volume (**6ca** (33.9%) vs **6da** (33.9%)). Changing the pyridine ligand from pyridine to 2-picoline in **6da** (33.9%) and **6db** (34.4%) also has little effect on the buried volume.

In an attempt to isolate complex **6fa** by crystallization from a solution of methylene chloride and excess pyridine, $(pyridine)_2Pd(2,6\text{-}Me_2C_6H_3)Br$ (**7**) was isolated instead of complex **6fa**. A similar product is formed when $((t\text{-}Bu)_3P)Pd(2\text{-}tol)Br$ is reacted with pyridine.[21] X-ray quality crystals of **7** were obtained, which allowed the structure to be confirmed as the *trans*-dipyridine complex (Figure S31). Observation of the reaction of complexes **3a**, **3c**, and **3d** with excess pyridine by ^{31}P NMR spectroscopy showed no evidence of displacement of PNp_3 by a second equivalent of pyridine. The decreased steric demand of PNp_3 compared to $P(t\text{-}Bu)_3$ likely results in a tighter coordination to palladium, preventing displacement by pyridine. The sterically demanding 2,6-dimethylphenyl ligand increases the lability of PNp_3, however, resulting in slow displacement of the phosphine in this case.

Steric Effects on the Cleavage Equilibrium. The effect of both the steric demand of the incoming pyridine ligand and the aryl ligand on the equilibrium constant could be evaluated independently in this study. For each of the dimer complexes (**3**), increasing steric hindrance of the pyridine resulted in a significant decrease in the binding equilibrium constant (Table 2). For example, complex **3a** with a sterically undemanding 4-tolyl aryl group reacted stoichiometrically with pyridine at all Pd/pyridine ratios. When complex **3a** was reacted with 2-picoline, the equilibrium constant was 3.8×10^2, which corresponds to at least a 2 orders of magnitude decrease in *K*. The equilibrium constant for 2,6-lutidine (5.8, **6ac**) was approximately 2 orders of magnitude less than for 2-picoline (**6ab**). Complexes **3c**, **3d**, and **3f** showed similar trends. The 2,6-lutidine complex could not be observed for these complexes even at high lutidine/Pd ratios. Whereas our results show that the steric demand of the pyridine derivative has a significant effect on the binding equilibria, prior studies with $[(Pr_3P)PdI_2]_2$ showed that the increased basicity of 2,6-lutidine compared to pyridine resulted in a larger equilibrium constant.[19b] Presumably, steric effects dominate in complexes **3a**−**3f** with the more sterically hindered PNp_3 and aryl ligands.

The steric demand of the aryl ligand also affects the equilibrium constant, although generally to a smaller extent. For all three pyridine derivatives, complex **3a** had a larger equilibrium constant than the complexes with *ortho*-substituents. With pyridine, the number or size of the *ortho*-substituent did not significantly impact the equilibrium constant, with **3c**, **3d**, and **3f** all giving similar values. With the more hindered 2-picoline, the number of *ortho* substituents did have a larger effect. The equilibrium constant for **3a** was 1 order of magnitude higher than that of the mono *ortho*-substituted complexes (**3c** and **3d**). The di-*ortho*-substituted complex **3f** had an equilibrium constant that was 3 orders of magnitude lower than that of **3c** or **3d**. In the case of 2,6-lutidine, only the unhindered complex **3a** was able to form an observable amount of adduct.

As noted above, complex **3f** is converted to a bis(pyridine) complex upon exposure to excess pyridine over an extended period. To ensure that this process did not affect the equilibrium values measured for **3f**, the rate of this process

Table 2. Equilibrium Constants (*K*) for the Reaction of 3 with Pyridine Derivatives to Afford 6[a]

5	3a	3c	3d	3f
pyridine	$>1 \times 10^4$ (**6aa**)[b]	$1.9 \pm 0.5 \times 10^2$ (**6ca**)	$4.6 \pm 2.4 \times 10^2$ (**6da**)	$1.2 \pm 0.3 \times 10^2$ (**6fa**)
2-picoline	$3.8 \pm 0.2 \times 10^2$(**6ab**)	15 ± 5 (**6cb**)	13 ± 0.6 (**6db**)	$8.6 \pm 3 \times 10^{-2}$ (**6fb**)
2,6-lutidine	5.8 ± 0.8 (**6ac**)	$<1 \times 10^{-3}$(**6cc**)[c]	$<1 \times 10^{-3}$(**6dc**)[c]	$<1 \times 10^{-3}$(**6 fc**)[c]

[a] $K = [6]^2/([3][5]^2)$ [b] 100% conversion to pyridine adduct was observed at all pyridine concentrations. [c] No lutidine adduct was observed.

DOI: 10.1021/acs.inorgchem.9b02164
Inorg. Chem. 2019, 58, 13299−13313

was followed by ^{31}P NMR spectroscopy. Complex **3f** (3.5 mM) was treated with pyridine (35 mM) in CH_2Cl_2 at room temperature. Immediately after the addition of pyridine, analysis by ^{31}P NMR spectroscopy showed that **3f** was completely consumed and the only resonance observed was that of $(PNp_3)Pd(2,6\text{-}Me_2C_6H_3)$(pyridine)Br (**6fa**, Scheme 1).

Scheme 1. Reaction of 3f with Pyridine to Give 7

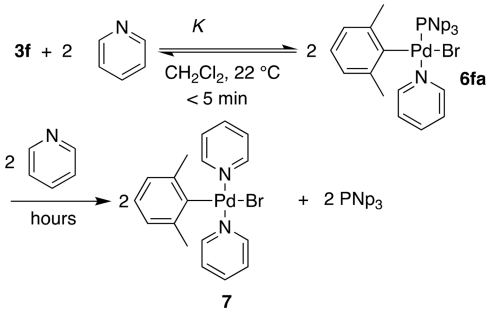

No free PNp_3 was observed, which indicates that no conversion to complex **7** had occurred in this time. After 14 h at room temperature, 16% of **6fa** was converted to bis(pyridine) complex **7** (Figure S58, Supporting Information). Heating the reaction to 60 °C for an additional 200 min resulted in 70% conversion of **6fa** to **7**. The rate of conversion of **6fa** to **7** is too slow at room temperature to affect the analysis of the equilibrium ratios in this study. Significantly, no free PNp_3 was observed in any of the equilibrium studies.

Coordination of Amines to Complex 3f. The reaction of the most sterically demanding palladium aryl dimer (**3f**) with amine substrates used in Buchwald–Hartwig reactions was next explored. We previously reported that bromide-bridged dimers related to **3a**–**3f** do not form a stable adduct with aniline, although they effectively catalyzed the arylation of aniline.[11] As expected, the reaction of dimer **3f** with an excess of aniline gave no evidence of formation of an aniline complex (**9a**) based on the ^{31}P NMR spectrum of the reaction mixture. Reaction of **3f** with the more basic amines, such as isobutyl amine (**8b**) or morpholine (**8c**) provides stable amine complexes (**9b**–**9c**, eq 4). Complex **9c** afforded X-ray quality

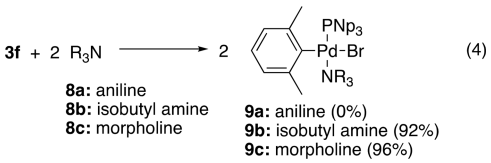

crystals that allowed confirmation of the structure as an adduct in which the morpholine coordinates as a neutral ligand (Figure 6). The amine coordinates *cis* to the aryl substituent as seen with the pyridine complexes.

Reaction of aniline with $[Pd(TNpP)Cl_2]_2$ (**10**)[9g] cleanly affords aniline complex **11** (eq 5). By replacing the 2,6-

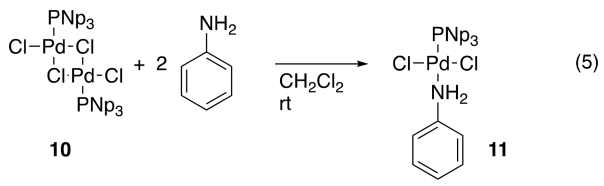

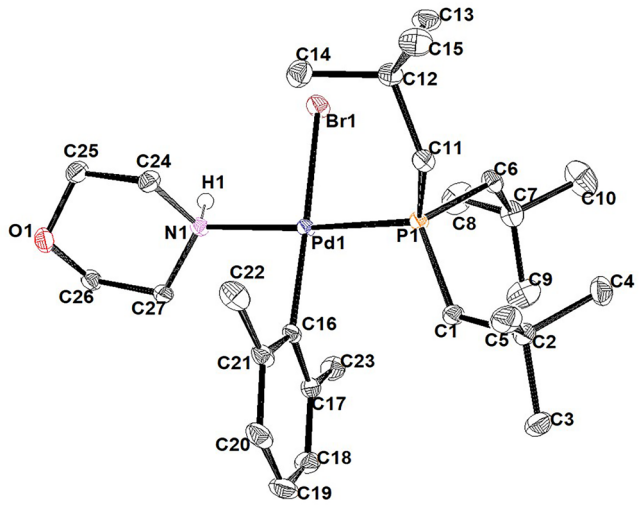

Figure 6. Thermal ellipsoid plot (50% probability) of the molecular structure of **9c**. Hydrogen atoms and disorder are omitted for clarity. Selected bond lengths (Å) and angles (deg): Pd1–N1, 2.1512(13); Pd1–Br1, 2.5322(2); Pd1–C16, 2.0147(16); Pd1–P1, 2.2818(4); N1–Pd1–Br1, 85.17(4); P1–Pd1–Br1, 94.220(12); N1–Pd1–P1, 173.00(4); C16–Pd1–Br1, 173.21(5); C16–Pd1–P1, 90.46(4); C16–Pd1–N1, 90.78(6).

dimethylphenyl substituent with the chloride, the palladium center is less sterically hindered and more electron-deficient. The more accessible and electron-deficient palladium center binds more readily to aniline than **3f**. Complex **11** gave X-ray quality crystals that allowed the structure to be determined (Figure S33). The solid state structure is a distorted square plane with a *trans* arrangement of the phosphine and amine ligands. As in **9b**, aniline coordinates as a neutral ligand.

Computational Results. Optimized geometries and vibrational frequencies for complexes **3** and **6** were calculated at the density functional theory[22] level with the B3LYP[23] exchange-correlation functional. The calculations used the DZVP2[24] basis set for the first and second row atoms (H, C, N, P), the DZVP[24] basis set for Br, and the pseudopotential (PP) based aug-cc-pVDZ-PP correlation-consistent basis set[25] for Pd. As shown in Tables 1 (**3a**–**3f**) and S10 (**6aa**–**6db**), the calculated structural parameters are in good agreement with experimental results. The Pd–Br, Pd–P, and Pd–N dative bonds are predicted to be 0.05 to 0.10 Å too long (on the order of up to 4%). This is typical of what is found in comparing the geometries of molecules with dative bonds to transition metal atoms using gradient corrected functionals with DFT. The calculated Pd–C covalent bond distances are in much better agreement with experimental results. The calculated and experimental bond angles are in agreement within a few degrees. The percent buried volumes obtained from DFT-optimized gas phase structures were consistently smaller (1.6–3°) than those obtained from solid-state structures but followed the same trends as those obtained from solid-state structures. The underestimation of the buried volume is likely due in part to the overestimation of the Pd–P bond length, which would decrease the steric interaction in the metal coordination sphere.

The calculated energetics using five different DFT functionals in both the gas phase and in solution for the dimer–monomer equilibrium (eq 6) reaction for different substituted aromatics are reported in Tables 3 and S29. The B3LYP results

DOI: 10.1021/acs.inorgchem.9b02164
Inorg. Chem. 2019, 58, 13299–13313

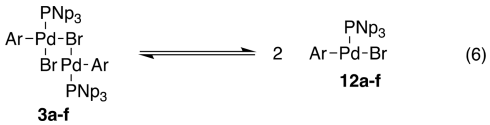

(6)

Table 3. Calculated Solution Phase (CH_2Cl_2) Bromine-Bridge Dissociation Reaction Free Energies for eq 6 at 298 K (kcal/mol)

Ar	B3LYP	M06	ωB97xD	B3LYP-D3BJ	B97D3BJ
C_6H_5 (**3g**)	−15.7	0.9	1.9	8.1	2.5
4-MeC_6H_4 (**3a**)	−10.8	7.8	8.7	14.4	8.4
4-*t*-BuC_6H_4 (**3b**)	−12.4	6.9	8.0	14.0	8.1
2-MeC_6H_4 (**3c**)	−14.0	2.7	4.4	10.4	4.7
2-*i*-PrC_6H_4 (**3g**)	−1.7	19.0	17.0	23.1	17.9
2-Me-4-$OMeC_6H_3$ (**3e**)	−16.4	0.3	1.7	7.7	2.3
2,6-$Me_2C_6H_3$(**3f**)	−15.3	1.3	2.9	9.1	3.2

predict that formation of the monomer (**12**) is always highly favored in dichloromethane solution, except for **3d**, where monomer formation is weakly favored. In contrast, dimer formation is always favored in the gas phase with the B3LYP functional (Table S29). The other four functionals, which are expected to handle the nonbonded van der Waals interactions in these sterically bulky systems in a more even manner, predict that dimer **3** is heavily preferred in the gas phase. The dimer is favored in solution, as well, for all four functionals, but with smaller energy differences. On the basis of the calculations, complexes **3g**, **3c**, **3e**, and **3f** may be in equilibrium with small concentrations of their corresponding monomer complexes in solution. Stable three-coordinate palladium aryl complexes have been characterized, but the known examples require highly sterically demanding ligands, such as tri-*tert*-butylphosphine or triadamantylphosphine.[26] On the basis of the observation of four stereoisomers for complexes **3c** and **3d** in solution,[10] complexes **3a**−**3f** are expected to exist primarily as halide-bridged dimers in solution.

The stability of dimer complexes **3a**−**3g** compared to the three-coordinate monomers **12a**−**12g** roughly follows the steric demand of the ligands, although there are exceptions to this trend. As expected, the endothermicity of dimer cleavage decreases going from 4-substituted (**3a**, **3b**) to 2-substituted (**3c**) to 2,6-disubstituted (**3f**) as the steric demand of the aryl ligand increases. Replacing the 2-methyl substituent in **3c** with isopropyl (**3d**) results in a significantly higher endothermicity, which is not expected based on steric effects. If an electron donating methoxy group is substituted at the 4- position in **3c** to form **3e**, the endothermicity is the smallest. This could reflect an increased *trans* effect from the more electron-rich aryl ring. Phenyl-substituted **3g** has a nearly identical value to **3e** and a much lower endothermicity than **3a** or **3b**, however. The tendency of the dimer to cleave appears to depend on several factors than cannot be clearly assigned to steric and/or electronic effects.

The solid-state structures of the pyridine complexes have a *cis* relationship between the pyridine and aryl ligand in each case. In solution, a single isomer was observed by ^{31}P NMR in all cases, except **6ab**, where two complexes were observed. We hypothesized that these may correspond to *cis* and *trans* isomers of **6ab**. The relative energies of the **6**-*cis* and **6**-*trans* isomers of the (Np_3P)Pd(pyr)(Ar)Br complexes were analyzed computationally using the B3LYP, M06, and ωB96xD functionals (eq 7, Tables 4 and S30). All three functionals

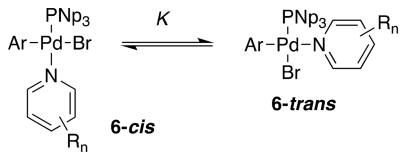

(7)

Table 4. Calculated *trans*−*cis* Free Energy Differences (eq 7) at 298 K in CH_2Cl_2 Solution (kcal/mol)

3	5	6	B3LYP	M06	ωB97xD
C_6H_5 (**3g**)	pyridine (**5a**)	**6ga**	2.5	2.0	1.9
	2-picoline (**5b**)	**6gb**	4.4	4.1	4.0
	2,6-lutidine (**5c**)	**6gc**	6.5	5.9	6.7
4-MeC_6H_4 (**3a**)	pyridine (**5a**)	**6aa**	1.4	−0.3	0.2
	2-picoline (**5b**)	**6ab**	5.5	4.7	5.3
	2,6-lutidine (**5c**)	**6ac**	9.3	7.5	9.4
2-MeC_6H_4 (**3c**)	pyridine (**5a**)	**6ca**	0.8	−0.1	0.5
	2-picoline (**5b**)	**6cb**	2.2	0.8	1.3
	2,6-lutidine (**5c**)	**6cc**	4.9	4.7	5.9
2-*i*-PrC_6H_4 (**3d**)	pyridine (**5a**)	**6da**	3.9	2.4	3.8
	2-picoline (**5b**)	**6db**	7.3	6.8	7.8
	2,6-lutidine (**5c**)	**6dc**	8.3	8.0	9.6
2,6-$Me_2C_6H_3$ (**3f**)	pyridine (**5a**)	**6fa**	3.1	2.1	3.1
	2-picoline (**5b**)	**6fb**	3.7	2.0	2.9
	2,6-lutidine (**5c**)	**6 fc**	2.4	0.7	2.6

gave similar predicted trends for the relative stabilities of the two isomers. In the gas phase, the **6**-*cis* isomer is predicted to be strongly favored for all complexes (Table S30). This trend is expected based on the preference for the strong *trans*-effect aryl ligand to be *trans* to the weak *trans*-effect bromide ligand. The *trans* isomer would also lead to increased steric strain between the PNp_3, aryl, and pyridine ligands. In solution, the **6**-*cis* isomer is predicted to be favored in nearly all cases, but by a smaller amount than in the gas phase. For complexes with zero or one *ortho* substituent (**6ax**, **6cx**, and **6dx**), the energy difference between the *cis* and *trans* isomers increases with increasing size of the pyridine ligand. For example, the *cis* and *trans* isomers of the 4-tolylpyridine complex (**6aa**) are calculated to be nearly thermoneutral in solution. In the case of the 2-picoline complex (**6ab**), the *cis* isomer is predicted to be approximately 5 kcal/mol more stable than the *trans* isomer in solution. The increased preference for the *cis* isomer is presumably due to the increased steric strain between 2-picoline and PNp_3 ligands in the **6**-*trans* isomer. The 2,6-dimethylphenyl complexes (**6fx**) are predicted to have a small decrease in energy differences between **6**-*cis* and **6**-*trans* isomers as the steric demand of the pyridine increases. This change in behavior likely reflects increased steric strain between the 2,6-dimethylphenyl and pyridine ligands that destabilize the **6**-*cis* isomer relative to the **6**-*trans* isomer.

The energetics for the equilibrium reaction of various pyridines with the three-coordinate monomer complex **12** (eq 8, Tables 5 and S31) and dimeric complex **3** (eq 9, Tables 6 and S32) were predicted using different DFT functionals in both the gas phase and CH_2Cl_2 solution. When attempts were made computationally to add pyridines to dimeric complex **3**, the pyridine ligand did not bind during the optimization. Thus, the reactions of dimers **3a**−**3g** with pyridines are predicted to

DOI: 10.1021/acs.inorgchem.9b02164
Inorg. Chem. 2019, 58, 13299−13313

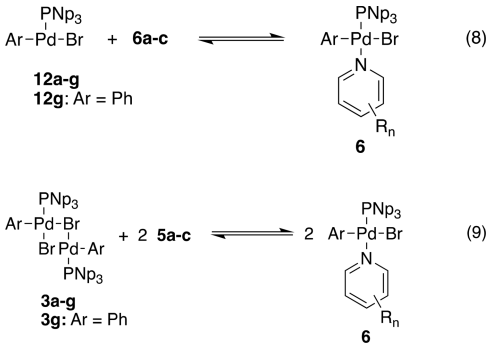

be dissociative processes. In contrast, previously studied systems are proposed to undergo dimer cleavage through an associative mechanism.[19,20] These systems used less-hindered complexes, such as $[Pd_2X_6]^{2-}$ and $[(n\text{-alkyl}_3P)PdX_2]_2$. The increased steric demand of complex **3** appears to prevent an associative mechanism.

For the reaction of pyridine with a 3-coordinate monopalladium complex (**12**, eq 8), four of the functionals predict the reactions to be exothermic in the gas phase and in solution except for the formation of **6fc** from 2,6-lutidine and **12f**. In contrast, the B3LYP functional predicts that pyridine coordination would be endothermic in all cases in solution.

Complexes **3a**−**3g** exist as halide bridged dimers in solution as shown above. Thus, the critical thermodynamics are the ones shown in Table 6 (eq 9), which can be derived by adding the dissociation values in Table 3 (eq 6) to twice the corresponding values in Table 5 (eq 8) as two pyridines will react with the two monomers that are formed. The ωB97xD functional tends to predict reaction energies that are too negative as compared to experimental results, but qualitative agreement with experimental results is found for most of the reaction energies in solution. The M06, B97D3BJ, and B3LYP-D3BJ functionals generally predict reaction free energies that are too positive as compared to experimental results, and again, qualitative agreement with experimental results is found for most of the reactions. The B3LYP energies are all much less negative than experimental results, and in general, all of the predicted reaction energies are positive. Thus, the experimental free energies are bracketed by the ωB97xD functional and by the M06, B97D3BJ, and B3LYP-D3BJ functionals.

Experimentally, the binding order is pyridine > 2-picoline > 2,6-lutidine for all complexes tested. For the reactions of **3a**, **3c**, and **3d**, excluding B3LYP, the order of reactivity is predicted to be 2-picoline > pyridine > 2,6-lutidine. B3LYP, on the other hand, predicts the correct order of reactivity, even though the actual reaction free energies are predicted to be too positive. For **3f**, all of the methods predict the correct reactivity order. The order of the gas phase basicity is pyridine < 2-picoline < 2,6-lutidine from experimental results, and the calculations match this order (Table S37). Thus, there is a balance between the basicity and the steric interactions governing the experimental ordering. B3LYP accounts for the least amount of steric interaction so its energetics are dominated by the basicity. However, the inability to account for the steric interactions leads to B3LYP's inability to predict the amount of binding resulting in free energies that are too positive. The other methods are able to predict the size of the steric interactions better than they do predict about the correct free energies but get some overbinding in terms of the steric interactions. Thus, the basicity plays too important a role in the calculated values.

The first step in the formation of dipyridine complex **7** (Scheme 1) is the cleavage of dimer **3f** and addition of 2 equiv of pyridine to give two **6fa** (eq 10). This reaction is predicted to be slightly too exothermic by −0.1 to −6.7 kcal/mol with all of the functionals (Table 6). The calculated geometry parameters for **7** are shown in Table S35, where they are compared to the experimental values. The calculated geometry parameters are in good agreement with experimental results with bond distances within better than 0.04 Å. The energetics for the second step (eq 11 and Tables 7 and S36) are exothermic by *ca.* −10 kcal/mol at the B3LYP level. This is due to the fact that there are fewer steric interactions in **7** than in **6fa** and B3LYP does not incorporate the nonbonded interactions of the PNp_3 group properly. The M06 functional predicts the reaction to be slightly endothermic consistent with the observation that **7** is formed. Whether eq 10 is exothermic or endothermic in solution is within the accuracy of the method. At the ωB97xD level, the reaction is predicted to be endothermic by ∼5 kcal/mol so that the nonbonded interactions are being too heavily weighted with this functional. This is consistent with the results in Table 6. Equation 11 is

Table 5. Calculated Solution (CH_2Cl_2) Reaction Free Energies at 298 K (kcal/mol) for the Reactions of Pyridines 5a−5c with (PNp_3)PdArBr (12a−12g; eq 7)

12	5	6	B3LYP	M06	ωB97xD	B3LYP-D3BJ	B97D3BJ
C_6H_5 (**12g**)	pyridine (**5a**)	**6ga**	6.8	−1.6	−4.2	−4.7	−1.5
	2-picoline (**5b**)	**6gb**	8.4	−3.0	−5.5	−5.9	−2.9
	2,6-lutidine (**5c**)	**6gc**	11.3	−2.9	−6.1	−6.5	−3.4
4-MeC_6H_4 (**12a**)	pyridine (**5a**)	**6aa**	6.1	−3.1	−5.8	−6.5	−2.9
	2-picoline (**5b**)	**6ab**	6.6	−5.4	−8.2	−9.0	−5.7
	2,6-lutidine (**5c**)	**6ac**	10.9	−4.0	−7.4	−7.8	−4.4
2-MeC_6H_4 (**12c**)	pyridine (**5a**)	**6ca**	7.9	−0.7	−3.8	−4.1	−0.9
	2-picoline (**5b**)	**6cb**	9.7	−1.7	−4.7	−5.0	−1.9
	2,6-lutidine (**5c**)	**6cc**	14.8	0.1	−3.4	−3.5	−0.4
2-*i*-PrC_6H_4 (**12d**)	pyridine (**5a**)	**6da**	0.6	−8.7	−10.6	−10.9	−7.8
	2-picoline (**5b**)	**6db**	2.6	−10.4	−11.9	−12.2	−9.2
	2,6-lutidine (**5c**)	**6dc**	9.7	−6.0	−8.1	−8.2	−5.3
2,6-$Me_2C_6H_3$ (**12f**)	pyridine (**5a**)	**6fa**	6.9	−1.2	−4.8	−5.2	−1.6
	2-picoline (**5b**)	**6fb**	10.7	0.4	−3.6	−4.2	−0.7
	2,6-lutidine (**5c**)	**6 fc**	19.7	6.1	2.3	1.5	4.7

DOI: 10.1021/acs.inorgchem.9b02164
Inorg. Chem. 2019, 58, 13299−13313

Table 6. Calculated and Experimental Solution (CH_2Cl_2) Reaction Free Energies at 298 K (kcal/mol) for the Reactions of Pyridines 5a−c with $[(PNp_3)PdArBr]_2$ (3a−g) (eq 8)

3	5	6	B3LYP	M06	ωB97xD	B3LYP-D3BJ	B97D3BJ	exptl[a]
C_6H_5 (**3g**)	pyridine (**5a**)	**6ga**	−2.1	−2.2	−6.6	−1.4	−0.5	
	2-picoline (**5b**)	**6gb**	1.0	−5.2	−9.1	−3.8	−3.3	
	2,6-lutidine (**5c**)	**6gc**	6.9	−4.9	−10.3	−5.0	−4.4	
4-MeC_6H_4 (**3a**)	pyridine (**5a**)	**6aa**	1.4	1.7	−2.9	1.5	2.6	< −5.5
	2-picoline (**5b**)	**6ab**	2.5	−3.0	−7.8	−3.6	−2.9	−4.9 ± 0.1
	2,6-lutidine (**5c**)	**6ac**	10.9	−0.1	−6.0	−1.1	−0.3	−1.0 ± 0.1
2-MeC_6H_4 (**3c**)	pyridine (**5a**)	**6ca**	1.9	1.2	−3.3	2.2	2.9	−3.1 ± 0.2
	2-picoline (**5b**)	**6cb**	5.5	−0.7	−5.0	0.4	0.9	−1.6 ± 0.3
	2,6-lutidine (**5c**)	**6cc**	15.6	2.9	−2.4	3.5	3.9	>4.1
2-*i*-PrC_6H_4 (**3d**)	pyridine (**5a**)	**6da**	−0.5	1.7	−4.2	1.3	2.3	−3.6 ± 0.4
	2-picoline (**5b**)	**6db**	3.6	−1.8	−6.9	−1.3	−0.5	−1.5 ± 0.1
	2,6-lutidine (**5c**)	**6dc**	17.7	7.1	0.8	6.6	7.4	>4.1
2,6-$Me_2C_6H_3$ (**3f**)	pyridine (**5a**)	**6fa**	−1.5	−1.1	−6.7	−1.2	−0.1	−2.8 ± 0.2
	2-picoline (**5b**)	**6fb**	6.1	2.1	−4.3	0.8	1.7	1.5 ± 0.2
	2,6-lutidine (**5c**)	**6 fc**	24.1	13.6	7.4	12.1	12.6	>4.1

[a]Calculated using equilibrium constants (K) reported in Table 3.

Table 7. Calculated Solution (CH_2Cl_2) Reaction Free Energies at 298 K (kcal/mol) for eq 10 and eq 11

method	eq 10	eq 11
B3LYP	−1.5	−10.4
M06	−1.1	1.1
ωB97xD	−6.7	4.8
B3LYP-D3BJ	−0.1	7.2
B97D3BJ	−1.2	8.2

even more endothermic with the B3LYP-D3BJ and B97D3BJ functionals showing that, again, they may be overestimating the stabilization due to nonbonded interactions.

3f + 2pyr → **26fa** (10)

26fa + 2pyr → 27 + $2PNp_3$ (11)

CONCLUSIONS

Structural analysis of trineopentylphosphine palladium complexes confirms that there is a significant degree of conformational flexibility in the trineopentylphosphine ligands that allows accommodation of other sterically demanding ligands in the coordination environment. There is a dramatic difference in the conformation of PNp_3 coordinated to two-coordinate palladium ($Pd(PNp_3)_2$) and the four-coordinate complexes discussed here (**3** and **6**). Within the four-coordinate complexes, the neopentyl ligands adjust their conformations to tolerate aryl ligands on palladium. Changes in the torsional angles of the neopentyl substituents (Pd−P−C-C) and the P−C−C bond angles are the primary responses to increased steric demand. In the case of a 2,6-dimethylphenyl substituent, the phosphine is pyramidalized to move the neopentyl groups further from the palladium center. These changes in conformation can be seen through buried volume calculations that show decreasing $\%V_b$ with increasing steric demand of the aryl ligand on palladium. In contrast to the significant effect of the *cis*-aryl ligand on the PNp_3 conformation, the ligand *trans* to the phosphine has less impact.

The binding equilibria for cleavage of the halide bridged dimers (**3**) by pyridine to give pyridine complexes (**6**) are dependent primarily on the steric demand of the incoming pyridine ligand and to a lesser extent the steric demand of the aryl group on palladium. These results are in contrast to previous studies with less hindered palladium centers in which the pyridine basicity was a more important factor in the binding equilibrium.[19b] To our knowledge, this is the first analysis of steric effects of ligand binding in complexes with sterically demanding ligands relevant to palladium-catalyzed cross-coupling. Electronic structure calculations suggest that this ligand substitution process occurs by a dissociative mechanism, rather than the associative process seen in other halide dimer cleavage reactions.[19,20] This conclusion is based on the fact that a pyridine adduct of the halide bridged dimers (**3**), which would be required in an associative mechanism, could not be found computationally.

Electronic structure calculations of these systems highlight that the choice of functional plays a critical role in obtaining energies that are consistent with experimental results. Calculations using B3LYP were generally least consistent with the experiment and the other basis sets used in this study. The poor performance of B3LYP is thought to be due to its handling of the extensive van der Waals interactions in these complexes. None of the functionals were able to accurately calculate ΔG within ±1 kcal/mol for all of the reactions of pyridine derivatives with the dimer complexes (**3**), although the ωB97xD and M06, B97D3BJ, and B3LYP-D3BJ functionals bracketed the experimental values. The agreement of the computational results with experimental results is reasonable considering the difficulty in calculating nonbonded interactions and solvent effects. An error of 1 to 3 kcal/mol in each component readily accounts for the differences between the calculated values and experimental results. All of the functionals except B3LYP overestimated the effect of pyridine basicity on the binding equilibria relative to the steric effect, resulting in predictions that 2-picoline would bind more favorably than pyridine.

EXPERIMENTAL SECTION

General Procedure and Materials. PNp_3,[27] $Pd(PNp_3)_2$,[10,28] **3b**,[10] **3c**,[10] **3f**,[11] $(COD)Pd(CH_2TMS)_2$,[29] and **10**[9g] were prepared according to literature procedures. Other reagents were purchased from commercial suppliers and used as received. Toluene was refluxed over sodium for an hour and freshly distilled before use. Methylene

DOI: 10.1021/acs.inorgchem.9b02164
Inorg. Chem. 2019, 58, 13299−13313

chloride was distilled from CaH_2 under nitrogen prior to use. Reactions were conducted under nitrogen double-manifold inert-atmosphere techniques, unless noted otherwise.

[(PNp$_3$)Pd(4-MeC$_6$H$_4$)Br]$_2$ (3a). Pd(PNp$_3$)$_2$ (97.3 mg, 0.164 mmol) and 4-bromotoluene (96.4 μL, 0.78 mmol) were mixed together in 10 mL toluene in a two-neck flask under N_2. The reaction mixture was stirred at 70 °C for 14 h. After cooling to RT, all the volatiles were pumped off, and the remaining solids were washed with pentane. Then, the collected solids were dissolved in hot toluene again. The solution was filtered while hot to remove insoluble Pd black solids. Removal of the solvent under a vacuum afforded a white solid (73.88 mg, 70%). ^{1}H NMR (500 MHz, C_6D_6, 283 K): δ 7.64 (d, J = 5.3 Hz, 4H), 6.93 (d, J = 5.8 Hz, 4H), 1.77 (d, J = 10.7 Hz, 12H), 1.37 (s) 1.27 (brs, 54H). ^{13}C NMR (125 MHz, C_6D_6, 295 K): δ 148.3, 135.5, 132.2, 108.0, 40.0, 33.5, 32.6, 31.4 (brm), 20.80. ^{31}P NMR (202.5 MHz, C_6D_6, 295 K): δ 7.78, 6.14 ppm (1:0.13).

[(PNp$_3$)Pd(2-iPrC$_6$H$_4$)Br]$_2$ (3d). Pd(PNp$_3$)$_2$ (110.2 mg, 0.185 mmol) and 1-bromo-2-isopropylbenzene (142.3 μL, 0.93 mmol) were mixed together in 10 mL of toluene in a two-neck flask under N_2. The reagent mixture was stirred at 70 °C for 14 h. After cooling to RT, all the volatiles were pumped off, and the remaining solids were washed with pentane. Then, the collected solids were dissolved in hot toluene. The solution was filtered while hot to remove insoluble Pd black solids. Removal of the solvent under a vacuum afforded a white solid (80.8 mg, 65%). ^{1}H NMR (500 MHz, C_6D_6, 283 K): δ 7.74 (m, 2H), 7.10−7.01 (m, 6H), 2.40−1.20 (m, 60H), 0.70 (s, 18H). ^{13}C NMR (125 MHz, C_6D_6, 295 K): δ 151.4 (s), 134.3, 134.2 (d, J_{C-P} = 18.7 Hz), 126.4, 126.3 (d, J_{C-P} = 15.0 Hz), 125.4, 124.3, 108.0, 41.6, 37.5, 33.1 (brs), 26.3, 26.2 (d, J_{C-P} = 12.5 Hz), 24.5, 24.4 (d, J_{C-P} = 12.5 Hz). ^{31}P NMR (202.5 MHz, C_6D_6, 295 K): δ 9.4, 9.2, 8.23, 8.18 ppm.

[(PNp$_3$)Pd(2-Me-4-OMeC$_6$H$_3$)Br]$_2$ (3e). Pd(PNp$_3$)$_2$ (61.6 mg, 0.104 mmol) and 4-bromo-3-methylanisole (88 μL, 0.62 mmol) were mixed together in 10 mL of toluene in a one-neck flask under N_2. The reagent mixture was stirred at 70 °C for 14 h. After cooling to RT, all the volatiles were pumped off, and the remaining solids were washed with pentane. Then, the collected solids were dissolved in hot toluene. The solution was filtered while hot to remove insoluble Pd black solids. Removal of the solvent under a vacuum afforded a white solid (35.8 mg, 64%). ^{1}H NMR (600 MHz, C_6D_6, 308.5 K): δ 7.54 (d, J = 2.2 Hz, 2H), 6.82 (s, 2H), 6.65 (d, J = 7.0 Hz, 2H), 3.40 (s, 6H), 2.98 (s, 6H), 1.71 (brs, 12H), 1.27 (brs, 54H). ^{13}C NMR (125 MHz, C_6D_6, 295 K): δ 157.9, 141.6, 133.9, 116.5, 116.4, 111.0, 54.8, 33.1, 32.5, 27.4, 22.7. ^{31}P NMR (202.5 MHz, C_6D_6, 295 K): δ 9.3, 9.3, 8.00, 7.95 ppm.

Representative Procedure for Equilibrium Study Experiments of [(PNp$_3$)PdArBr]$_2$ and Pyridine Derivatives. [(PNp$_3$)Pd(2-iPrC$_6$H$_4$)Br]$_2$ (**3d**, 17.6 mg, 1.31 × 10^{-5} mol) was dissolved in methylene chloride in a 2.0 mL volumetric flask with the addition of the standard trimethyl phosphate (8.0 μL, 6.84 × 10^{-5} mol), which worked as the stock solution. The stock solution of **3d** (500 μL, 6.55 × 10^{-6} mol) and pyridine (10.6 μL, 1.31 × 10^{-5} mol) was transferred into an NMR tube. The resulting solution was allowed to stand for at least 5 min and then analyzed by ^{31}P NMR spectroscopy. Equilibrium constants were calculated according to the integration of ^{31}P signals (see calculation details in Supporting Information). The pyridine complexes (**6**) reverted to equilibrium mixtures of **3x**, **5x**, and **6xx** in the absence of excess pyridine ligand, so they were only characterized by ^{31}P NMR. In the case of **6aa**, **6ca**, **6da**, and **6db**, X-ray quality crystals were obtained upon crystallization from solutions containing excess pyridine or 2-picoline.

(PNp$_3$)Pd((CH$_3$)$_2$CHCH$_2$NH$_2$)(2,6-Me$_2$C$_6$H$_3$)Br (9b). **3f** (50 mg, 0.047 mmol) was dissolved in methylene chloride (6 mL). Then, isobutylamine (10.0 μL, 0.101 mmol) was added into the solution. After stirring for 1 h, the volatiles were removed under a vacuum to provide a white solid (52 mg, 92%). ^{1}H NMR (500 MHz, C_6D_6, 295 K): δ 6. 90 (m, 3H), 2.86 (s, 6H), 2.75 (brs, 2H), 2.27 (s, 4H), 2.23 (br, 1H), 2.03 (brs, 2H), 1.56 (brs, 18H), 1.36 (br, 6H), 0.93 (br, 2H), 0.78 (brs, 9H). ^{13}C NMR (125 MHz, C_6D_6, 295 K): δ 159.7, 140.2, 126.9, 124.6, 52.1, 43.9, 33.3 (d, J_{C-P} = 35 Hz), 30.2, 27.0, 19.5. ^{31}P{^{1}H} NMR (202.5 MHz, C_6D_6, 295 K): δ 16.9.

(PNp$_3$)Pd(morpholine)(2,6-Me$_2$C$_6$H$_3$)Br (9c). **3f** (70 mg, 0.065 mmol) was dissolved in methylene chloride (8 mL). Then, morpholine (13.0 μL, 0.150 mmol) was added into the solution. After stirring for 1 h, the volatiles were removed under a vacuum to provide a white solid (78 mg, 96%). Colorless single crystals were formed after slow evaporation of a benzene solution. ^{1}H NMR (500 MHz, C_6D_6, 295 K): δ 7.05−6.93 (m, 1H), 6.88 (d, J = 7.2 Hz, 2H), 3.59 (br, 1H), 3.08 (d, J = 12.5 Hz, 2H), 2.83 (s, 6H), 2.73 (m, 6 H), 2.68 (m, 2 H), 2.02 (brs, 2H), 1.54 (s, 18 H), 1.36 (s, 4H), 0.76 (s, 9H). ^{13}C NMR (125 MHz, C_6D_6, 295 K): δ 160, 140.0, 127.0, 124.6, 67.8, 49.4, 43.9 (d, J_{C-P}= 9.7 Hz), 33.3, 32.8, 26.9. ^{31}P{^{1}H} NMR (202.5 MHz, C_6D_6, 295 K): δ 12.0

(PNp$_3$)Pd(C$_6$H$_7$N)Cl$_2$ (11). [(PNp$_3$)PdCl$_2$]$_2$ (100 mg, 0.119 mmol) was dissolved in methylene chloride (8 mL). Then, aniline (32.3uL, 0.357 mmol) was added into the solution. After stirring for 1 h, the volatiles were removed under a vacuum to provide an orange solid (116.4 mg, 95%). Orange single crystals were formed after slow evaporation of a benzene solution. ^{1}H NMR (500 MHz, C_6D_6, 295 K): δ 7.24 (d, J = 7.8 Hz, 2H), 7.00 (t, J = 7.8 Hz, 2H), 6.85 (t, J = 7.3 Hz, 1H), 3.82 (s, 2H), 2.12 (d, J = 12.8 Hz, 6H), 1.20 (s, 27 H). ^{13}C NMR (125 MHz, C_6D_6, 295 K): δ 141.4, 129.1, 124.4, 121.3, 38.6 (d, J_{C-P}= 25.2 Hz), 33.2 (d, J_{C-P} = 6.4 Hz), 32.4 (d, J_{C-P} = 4.3 Hz). ^{31}P{^{1}H} NMR (202.5 MHz, C_6D_6, 295 K): δ 15.5.

X-ray Crystallography. Crystals of appropriate dimension were mounted on Mitgen cryoloops or a glass filament in a random orientation. Preliminary examination and data collection for complexes **3a**, **3e**, **6aa**, **6ab**, **6da**, **6db**, and **7** were performed on a Bruker Apex2 CCD-based X-ray diffractometer equipped with an Oxford N-Helix Cryosystem and fine focus Mo-target X-ray tube (λ = 0.71073 Å) operated at 1500 W of power (50 kV, 30 mA). The X-ray intensities were measured at 223(2) K; the detector was placed at a distance 6.000 cm from the crystal. The frames were integrated with the Saint software package[30] using a narrow-frame algorithm. Data were corrected for absorption effects using the multiscan method in SADABS. The space group was assigned by using XPREP of the Bruker ShelXTL package,[31] solved with ShelXT and refined with ShelXL 2014/7[32] and the graphical interface ShelXle.[33] All non-hydrogen atoms were refined anisotropically. H atoms attached to carbon were positioned geometrically and constrained to ride on their parent atoms.

Preliminary examination and data collection for complexes **9b** and **11** were performed using a Rigaku XtaLAB Synergy R, a DW system, and a HyPix diffractometer operating at T = 100.00(10) K. Data were measured using ω scans using Mo Kα radiation. The total number of runs and images was based on the strategy calculation from the program CrysAlisPro, and the unit cell was refined using CrysAlisPro.[34] Data reduction, scaling and absorption corrections were performed using CrysAlisPro. The structure was solved and the space group determined by the ShelXT[35] structure solution program using intrinsic phasing methods and refined by least-squares using version 2018/3 of ShelXL[36] and graphical interface Olex2.[37] All non-hydrogen atoms were refined anisotropically. H atoms attached to carbon were positioned geometrically and constrained to ride on their parent atoms.

The structure of [(PNp$_3$)Pd(4-MeC$_6$H$_4$)Br]$_2$ (**3a**) was found to contain multiple two-component disorders. Within the asymmetric unit, two symmetrically independent molecules were found. In molecule one (containing a Pd1−Pd2−Br1−Br2 core), "rotation" two-component disorders were found at both of the two neopentyl ligands. In molecule two (containing Pd3−Br3A), three sites were disordered. A two component disorder was found at the 4-tolyl ligand, within which three pairs of the equivalent atoms of the two moieties (C45 and C45A; C50 and C50A; C51 and C51A) were constrained to have identical ADPs (EADP). Disorder was also found at the site of Br3A and Br3B. The bonds of Pd3−Br3A and Pd3−Br3B were restrained to have similar distances (SADI). The third disorder in this molecule was located at the neopentyl ligand. It was modeled as a "rotation" two-component disorder (C1−C2−C3 vs C1A−C2A−C3A). Equivalent bonds of the two moieties were restrained to have similar bond distances (SADI).

DOI: 10.1021/acs.inorgchem.9b02164
Inorg. Chem. 2019, 58, 13299−13313

The structure of $(PNp_3)Pd(2\text{-}MeC_6H_3)(Pyr)Br$ (**6ab**) was also found to have a two-component "ring flipping" disorder at the 2-tolyl ligand. Within these moieties, atoms were subjected to a rigid bond restraint (RIGU). The two disordered components were restrained to have similar geometries (SAME command of ShelXL).

The structure of $(PNp_3)Pd(2\text{-}i\text{-}PrC_6H_4)_2(2\text{-picoline})Br$ (**6db**) was found to have a two-component "ring flipping" disorder at the 2-picoline ligand. Within these moieties, atoms were subjected to a rigid bond restraint (RIGU). Also, as C10 and C10B appeared unstable when refined anisotropically, they were treated approximately as isotropic (ISOR).

The structure of $(PNp_3)Pd(2,6\text{-}Me_2C_6H_3)(morpholine)Br$ (**9b**) was found to have a positional disorder on the morpholine ligand at one of the two molecules in the asymmetric unit. The structure was successfully modeled by two moieties with an occupancy ratio of 0.6:0.4.

The structure of $(PNp_3)Pd(aniline)Cl_2$ (**11**) was found to have a rotational disorder on one of the neopentyl ligands. Atoms on the two moieties were restrained to have similar geometries (SAME).

Computational Methods. The geometries were optimized, and vibrational frequencies were calculated at the density functional DFT[22] level with the B3LYP[23] exchange-correlation functional. Vibrational frequencies were predicted to ensure that the optimized structures were minima. The calculations used the DZVP2[24] basis set for the first and second row atoms (H, C, N, P), the DZVP[24] basis set for Br, and the pseudopotential (PP)-based aug-cc-pVDZ-PP correlation-consistent basis set[25] for Pd. Single point M06[38] and ωB97xD[39] calculations were done at the B3LYP optimized geometries. The gas phase calculations were performed using the Gaussian 09 program system.[40] Calculations in CH_2Cl_2 solution (ε = 2.02) were performed using a self-consistent reaction field approach[41] with the COSMO parameters[41,42] using Gaussian 03.[43] Additional single point B3LYP and B97D3 calculations using the D3 version of Grimme's dispersion with Becke-Johnson damping[44] (will be named as B3LYP-D3BJ and B97D3BJ)[45] were performed using cc-pVDZ for H;[46] aug-cc-pVDZ for C, N,[47] and P;[48] aug-cc-pVDZ-PP for Br;[49] and cc-pVDZ-PP for Pd as basis sets. The solvation COSMO calculations were redone using the new basis sets with B3LYP-D3BJ as a functional. This additional set of calculation was performed using Gaussian 16.[50] The Gibbs free energy in CH_2Cl_2 solution at 298 K was calculated from eq 12:

$$\Delta G_{sol} = \Delta G_{gas} + \Delta G_{solv} \quad (12)$$

where ΔG_{gas} is the gas phase free energy at 298 K and ΔG_{solv} is the CH_2Cl_2 solvation free energy at 298 K. The solvation energy is only the electrostatic term (polarized solute − solvent).

Calculation of %V_b. Percent buried volumes for the complexes were calculated using the SambVca 2.0 Web Application.[16] The metal was defined as the center of the sphere, and the P of the ligand being analyzed was used to define the z axis. The following default parameters were used for all calculations: atomic radii were the bond radii table scaled by 1.17 in the application, sphere radius = 3.5 Å, mesh spacing = 0.1 Å, and H atoms were excluded from the calculations.

■ ASSOCIATED CONTENT

Supporting Information

The Supporting Information is available free of charge on the ACS Publications website at DOI: 10.1021/acs.inorgchem.9b02164.

NMR spectra of isolated complexes, X-ray crystallography data, data for pyridine binding experiments, reaction profile for the addition of pyridine to **3f**, additional reaction energies, proton affinities of the pyridines, Cartesian coordinates in angstroms for optimized DFT geometries (PDF)

Accession Codes

CCDC 1941334−1941342 contain the supplementary crystallographic data for this paper. These data can be obtained free of charge via www.ccdc.cam.ac.uk/data_request/cif, by emailing data_request@ccdc.cam.ac.uk, or by contacting The Cambridge Crystallographic Data Centre, 12 Union Road, Cambridge CB2 1EZ, UK; fax: + 44 1223 336033.

■ AUTHOR INFORMATION

Corresponding Authors

*E-mail: dadixon@ua.edu.
*E-mail: kshaughn@ua.edu.

ORCID

Monica Vasiliu: 0000-0001-7573-4787
Fengrui Qu: 0000-0002-9975-2573
Deidra L. Gerlach: 0000-0002-1246-1192
David A. Dixon: 0000-0002-9492-0056
Kevin H. Shaughnessy: 0000-0002-1375-5563

Notes

The authors declare no competing financial interest.

■ ACKNOWLEDGMENTS

Acknowledgment is made to the National Science Foundation (CHE-1058984) for partial financial support of the experimental work. Structures of **9b** and **11** were obtained on an X-ray diffractometer purchased with support from NSF (CHE MRI 1828078). Johnson-Matthey is acknowledged for donation of palladium salts. The computational work was supported by the Chemical Sciences, Geosciences, and Biosciences Division, Office of Basic Energy Sciences, U.S. Department of Energy (DOE) under the Catalysis Center Program by a subcontract from the Pacific Northwest National Laboratory (KC0301050-47319). D.A.D. also thanks the Robert Ramsay Chair Fund of The University of Alabama for support.

■ REFERENCES

(1) Surry, D. S.; Buchwald, S. L. Dialkylbiaryl phosphines in Pd-catalyzed amination: a user's guide. *Chem. Sci.* **2011**, *2*, 27−50.

(2) Fleckenstein, C. A.; Plenio, H. Sterically demanding trialkylphosphines for palladium-catalyzed cross coupling reactions-alternatives to $PtBu_3$. *Chem. Soc. Rev.* **2010**, *39*, 694−711.

(3) (a) Grasa, G. A.; Colacot, T. J. α-Arylation of Ketones using Highly Active, Air-Stable $(DtBPF)PdX_2$ (X = Cl, Br) Catalysts. *Org. Lett.* **2007**, *9*, 5489−5492. (b) Hartwig, J. F. Evolution of a Fourth Generation Catalyst for the Amination and Thioetherification of Aryl Halides. *Acc. Chem. Res.* **2008**, *41*, 1534−1544.

(4) (a) Valente, C.; Çalimsiz, S.; Hoi, K. H.; Mallik, D.; Sayah, M.; Organ, M. G. The Development of Bulky Palladium NHC Complexes for the Most-Challenging Cross-Coupling Reactions. *Angew. Chem., Int. Ed.* **2012**, *51*, 3314−3332. (b) Valente, C.; Pompeo, M.; Sayah, M.; Organ, M. G. Carbon-Heteroatom Coupling Using Pd-PEPPSI Complexes. *Org. Process Res. Dev.* **2014**, *18*, 180−190. (c) Izquierdo, F.; Manzini, S.; Nolan, S. P. The use of the sterically demanding IPr* and related ligands in catalysis. *Chem. Commun.* **2014**, *50*, 14926−14937.

(5) (a) Ehrentraut, A.; Zapf, A.; Beller, M. A new improved catalysts for the palladium catalyzed amination of aryl chlorides. *J. Mol. Catal. A: Chem.* **2002**, *182*−*183*, 515−523. (b) Rodriguez, S.; Qu, B.; Haddad, N.; Reeves, D. C.; Tang, W.; Lee, H.; Krishnamurthy, D.; Senanayake, C. H. Oxaphosphole-Based Monophosphorus Ligands for Palladium-Catalyzed Amination Reactions. *Adv. Synth. Catal.* **2011**, *353*, 533−537.

DOI: 10.1021/acs.inorgchem.9b02164
Inorg. Chem. 2019, 58, 13299−13313

(6) (a) Organ, M. G.; Abdel-Hadi, M.; Avola, S.; Dubovyk, I.; Hadei, N.; Kantchev, E. A. B.; O'Brien, C. J.; Sayah, M.; Valente, C. Pd-catalyzed aryl amination mediated by well defined, N-heterocyclic carbene (NHC)-Pd precatalysts, PEPPSI. *Chem. - Eur. J.* **2008**, *14*, 2443−2452. (b) Tu, T.; Fang, W.; Jiang, J. A highly efficient precatalyst for amination of aryl chlorides: synthesis, structure and application of a robust acenaphthoimidazolylidene palladium complex. *Chem. Commun.* **2011**, *47*, 12358−12360. (c) Chartoire, A.; Frogneux, X.; Boreux, A.; Slawin, A. M. Z.; Nolan, S. P. [Pd(IPr*)(3-Cl-pyridinyl)Cl_2]: A Novel and Efficient PEPPSI Precatalyst. *Organometallics* **2012**, *31*, 6947−6951. (d) Meiries, S.; Chartoire, A.; Slawin, A. M. Z.; Nolan, S. P. [Pd(IPr*)(acac)Cl]: An easily synthesized, bulky precatalyst for C-N bond formation. *Organometallics* **2012**, *31*, 3402−3409. (e) Zhu, L.; Ye, Y.-M.; Shao, L.-X. Well-defined NHC-Pd(II)-Im (NHC = N-heterocyclic carbene; Im = 1-methylimidazole) complex catalyzed C-N coupling of primary amines with aryl chlorides. *Tetrahedron* **2012**, *68*, 2414−2420. (f) Bastug, G.; Nolan, S. P. [Pd(IPr*OMe)(cin)Cl] (cin = Cinnamyl): A Versatile Catalyst for C-N and C-C Bond Formation. *Organometallics* **2014**, *33*, 1253−1258. (g) Lan, X.-B.; Li, Y.; Li, Y.-F.; Shen, D.-S.; Ke, Z.; Liu, F.-S. Flexible Steric Bulky Bis(Imino)-acenaphthene (BIAN)-Supported N Heterocyclic Carbene Palladium Precatalysts: Catalytic Application in Buchwald-Hartwig Amination in Air. *J. Org. Chem.* **2017**, *82*, 2914−2925.

(7) (a) Urgaonkar, S.; Verkade, J. G. Scope and limitations of $Pd_2(dba)_3$/P(*i*-$BuNCH_2CH_2)_3N$-catalyzed Buchwald-Hartwig amination reactions of aryl chlorides. *J. Org. Chem.* **2004**, *69*, 9135−9142. (b) Reddy, C. V.; Kingston, J. V.; Verkade, J. G. (*t*-Bu)$_2$PN = P(*i*-$BuNCH_2CH_2)_3N$: new efficient ligand for palladium-catalyzed C-N couplings of aryl and heteroaryl bromides and chlorides and for vinyl bromides at room temperature. *J. Org. Chem.* **2008**, *73*, 3047−3062.

(8) Lee, D.-H.; Taher, A.; Hossain, S.; Jin, M.-J. An efficient and general method for the Heck and Buchwald-Hartwig coupling reactions of aryl chlorides. *Org. Lett.* **2011**, *13*, 5540−5543.

(9) (a) Hill, L. L.; Moore, L. R.; Huang, R.; Craciun, R.; Vincent, A. J.; Dixon, D. A.; Chou, J.; Woltermann, C. J.; Shaughnessy, K. H. Bulky alkylphosphines with neopentyl substituents as ligands in the amination of aryl bromides and chlorides. *J. Org. Chem.* **2006**, *71*, 5117−5125. (b) Hill, L. L.; Smith, J. M.; Brown, W. S.; Moore, L. R.; Guevera, P.; Pair, E. S.; Porter, J.; Chou, J.; Wolterman, C. J.; Craciun, R.; Dixon, D. A.; Shaughnessy, K. H. Neopentylphosphines as effective ligands in palladium-catalyzed cross-couplings of aryl bromides and chlorides. *Tetrahedron* **2008**, *64*, 6920−6934. (c) Hill, L. L.; Crowell, J. L.; Tutwiler, S. L.; Massie, N. L.; Hines, C. C.; Griffin, S. T.; Rogers, R. D.; Shaughnessy, K. H.; Grasa, G. A.; Johansson Seechurn, C. C. C.; Li, H.; Colacot, T. J.; Chou, J.; Woltermann, C. J. Synthesis and X-Ray Structure Determination of Highly Active Pd(II), Pd(I) and Pd(0) Complexes of Di-(*tert*-butyl)neopentylphosphine (DTBNpP) in the Arylation of Amines and Ketones. *J. Org. Chem.* **2010**, *75*, 6477−6488. (d) Raders, S. M.; Jones, J. M.; Semmes, J. G.; Kelley, S. P.; Rogers, R. D.; Shaughnessy, K. H. Di-*tert*-butylneopentylphosphine (DTBNpP): An Efficient Ligand in the Palladium-Catalyzed α-Arylation of Ketones. *Eur. J. Org. Chem.* **2014**, *2014*, 7395−7404. (e) Semmes, J. G.; Bevans, S. L.; Mullins, H. C.; Shaughnessy, K. H. Arylation of diethyl malonate and ethyl cyanoacetate catalyzed by palladium/di-*tert*-butylneopentylphosphine. *Tetrahedron Lett.* **2015**, *56*, 3447−3450. (f) Lauer, M. G.; Thompson, M. K.; Shaughnessy, K. H. Controlling Olefin Isomerization in the Heck Reaction with Neopentyl Phosphine Ligands. *J. Org. Chem.* **2014**, *79*, 10837−10848. (g) Barnett, K. L.; Howard, J. R.; Treager, C. J.; Shipley, A. T.; Stullich, R. M.; Qu, F.; Gerlach, D. L.; Shaughnessy, K. H. Air-Stable [(R_3P)$PdCl_2$]$_2$ Complexes of Neopentylphosphines as Cross-Coupling Precatalysts: Catalytic Application and Mechanism of Catalyst Activation and Deactivation. *Organometallics* **2018**, *37*, 1410−1424.

(10) Raders, S. M.; Moore, J. N.; Parks, J. K.; Miller, A. D.; Leißing, T. M.; Kelley, S. P.; Rogers, R. D.; Shaughnessy, K. H. Trineopentylphosphine: A Conformationally Flexible Ligand for the Coupling of Sterically Demanding Substrates in the Buchwald-Hartwig Amination and Suzuki-Miyaura Reaction. *J. Org. Chem.* **2013**, *78*, 4649−4664.

(11) Hu, H.; Qu, F.; Gerlach, D. L.; Shaughnessy, K. H. Mechanistic Study of the Role of Substrate Steric Effects and Aniline Inhibition on the Bis(trineopentylphosphine)palladium(0)-Catalyzed Arylation of Aniline Derivatives. *ACS Catal.* **2017**, *7*, 2516−2527.

(12) (a) Calvin, G.; Coates, G. E. Organopalladium compounds. *J. Chem. Soc.* **1960**, 2008−2016. (b) Bartolomé, C.; Espinet, P.; Villafañe, F.; Giesa, S.; Martín, A.; Orpen, A. G. (2,4,6-Tris-(trifluoromethyl)phenyl)palladium(II) Complexes. *Organometallics* **1996**, *15*, 2019−2028. (c) Bartolomé, C.; Espinet, P.; Martín-Alvarez, J. M.; Villafañe, F. Monoarylated Fluoromesitylpalladium Complexes. *Eur. J. Inorg. Chem.* **2003**, *2003*, 3127−3138. (d) Jun, H.; Young, V. G., Jr.; Angelici, R. J. A phosphorus analog (C:P-) of a bridging cyanide (C:N-) ligand: synthesis and structure of (Cl)-(PEt_3)$_2$Pt(μ-C≡P)Pt(PEt_3)$_2$. *J. Am. Chem. Soc.* **1992**, *114*, 10064−5.

(13) (a) Wakioka, M.; Nakamura, Y.; Wang, Q.; Ozawa, F. Direct Arylation of 2-Methylthiophene with Isolated [PdAr(μ-O_2CR)-(PPh_3)]n Complexes: Kinetics and Mechanism. *Organometallics* **2012**, *31*, 4810−4816. (b) Qian, R.; Liao, Y.-X.; Guo, Y.-L.; Guo, H. ESI-FTICR-MS Studies on Gas Phase Fragmentation Reactions of ArPd(PPh_3)$_2$I Complexes. *J. Am. Soc. Mass Spectrom.* **2006**, *17*, 1582−1589.

(14) Paul, F.; Patt, J.; Hartwig, J. F. Structural characterization and simple synthesis of {Pd[P(*o*-tol)$_3$]$_2$}, dimeric palladium (II) complexes by oxidative addition of aryl bromides, and corresponding monometallic amine complexes. *Organometallics* **1995**, *14*, 3030−3039.

(15) Chaudhari, K. R.; Wadawale, A. P.; Jain, V. K. Isolation of chloro-bridged arylpalladium complexes, [Pd_2Ar_2(μ-Cl)$_2$(PR_3)$_2$], in palladium catalyzed C-C cross coupling reaction of triarylbismuth with arylhalides. *J. Organomet. Chem.* **2012**, *698*, 15−21.

(16) Falivene, L.; Credendino, R.; Poater, A.; Petta, A.; Serra, L.; Oliva, R.; Scarano, V.; Cavallo, L. SambVca 2. A Web Tool for Analyzing Catalytic Pockets with Topographic Steric Maps. *Organometallics* **2016**, *35*, 2286−2293.

(17) (a) Bartell, L. S.; Bradford, W. F. Molecular structures of neopentane and di-tert-butylmethane by vapor-phase electron diffraction. *J. Mol. Struct.* **1977**, *37*, 113−126. (b) Cheng, M.-F.; Li, W.-K. Structural and Energetics Studies of Tri- and Tetra-*tert*-butylmethane. *J. Phys. Chem. A* **2003**, *107*, 5492−5498. (c) Liedle, S.; Oberhammer, H.; Allinger, N. L. The gas-phase structures of some highly strained compounds: di-*t*-butylmethane, di-*t*-butylamine and di-*t*-butyl ketone. *J. Mol. Struct.* **1994**, *317*, 69−75. (d) Ermer, O.; Bödecker, C.-D. Structure of di-1-adamantylmethane (DAM) and di-*tert*-butylmethane (DTBM). *Chem. Ber.* **1981**, *114*, 652−659.

(18) Weiss, I.; Oberhammer, H.; Gard, G. L.; Winter, R.; Seppelt, K. The molecular structure of bis(pentafluorosulfur)methane $(SF_5)_2CH_2$ and perfluorovinylsulfur pentafluoride $SF_5CF = CF_2$. *J. Mol. Struct.* **1992**, *269*, 197−205.

(19) (a) Pearson, R. G.; Muir, M. M. Rates of Cleavage of Halogen-Bridged Complexes of Platinum(II). *J. Am. Chem. Soc.* **1966**, *88*, 2163−2166. (b) Cusumano, M.; Giannetto, A.; Ficarra, P.; Ficarra, R.; Tommasini, S. Metal complexes of benzodiazepines. Part 2. The reaction of 1,4-benzodiazepines with halide-bridged complexes of palladium(II) [Pd_2X_4(PPr_3)$_2$] (X - Cl or I). *J. Chem. Soc., Dalton Trans.* **1991**, 1581−1584. (c) Ryabov, A. D.; Kuz'mina, L.; Polyakov, V. A.; Kazankov, G. M.; Ryabova, E. S.; Pfeffer, M.; van Eldik, R. Kinetics and mechanism of halogen-bridge cleavage in dimethylaminomethylphenyl-C^1,N pallada- and platinacycles by pyridines. Pressure effects, and crystal structures of the *N,N-cis* reaction product, its *N,N-trans* orthometallated analog and a dimer of similar reactivity. *J. Chem. Soc., Dalton Trans.* **1995**, 999−1006.

(20) (a) Muir, M. M.; Cancio, E. M. Mechanisms of Reactions of Binuclear Complexes. I. Cleavage by Olefins of a Halogen-Bridged Complex of Platinum(II). *Inorg. Chim. Acta* **1970**, *4*, 565−567. (b) Otto, S.; Roodt, A.; Elding, L. I. Bridge-splitting kinetics, equilibria and structures of *trans*-biscyclooctene complexes of platinum(II). *Dalton Trans* **2003**, 2519−2525.

DOI: 10.1021/acs.inorgchem.9b02164
Inorg. Chem. 2019, 58, 13299−13313

(21) Shen, Q.; Shekhar, S.; Stambuli, J. P.; Hartwig, J. F. Highly reactive, general, and long-lived catalysts for coupling heteroaryl and aryl chlorides with primary nitrogen nucleophiles. *Angew. Chem., Int. Ed.* **2005**, *44*, 1371−1375.
(22) Parr, R. G.; Yang, W. *Density Functional Theory of Atoms and Molecules*; Springer-Verlag: New York, 1989.
(23) (a) Becke, A. D. Density functional thermochemistry. III. The role of exact exchange. *J. Chem. Phys.* **1993**, *98*, 5648−5652. (b) Lee, C.; Yang, W.; Parr, R. G. Development of the Colle-Salvetti correlation-energy formula into a functional of the electron density. *Phys. Rev. B: Condens. Matter Mater. Phys.* **1988**, *37*, 785−789.
(24) Godbout, N.; Salahub, D. R.; Andzelm, J.; Wimmer, E. Optimization of Gaussian-type basis sets for local spin density functional calculations. Part I. Boron through neon, optimization technique and validation. *Can. J. Chem.* **1992**, *70*, 560−571.
(25) (a) Peterson, K. A.; Figgen, D.; Dolg, M.; Stoll, H. Energy-consistent relativistic pseudopotentials and correlation consistent basis sets for the 4d elements Y-Pd. *J. Chem. Phys.* **2007**, *126*, 124101. (b) Figgen, D.; Peterson, K. A.; Dolg, M.; Stoll, H. Energy-consistent pseudopotentials and correlation consistent basis sets for the 5d elements Hf-Pt. *J. Chem. Phys.* **2009**, *130*, 164108.
(26) (a) Stambuli, J. P.; Bühl, M.; Hartwig, J. F. Synthesis, characterization, and reactivity of monomeric arylpalladium halide complexes with a hindered phosphine as the only dative ligand. *J. Am. Chem. Soc.* **2002**, *124*, 9346−9347. (b) Stambuli, J. P.; Incarvito, C. D.; Bühl, M.; Hartwig, J. F. Synthesis, structure, theoretical studies, and ligand exchange reactions of monomeric, T-shaped arylpalladium-(II) halide complexes with an additional, weak agostic interaction. *J. Am. Chem. Soc.* **2004**, *126*, 1184−1194. (c) Chen, L.; Francis, H.; Carrow, B. P. An "On-Cycle" Precatalyst Enables Room-Temperature Polyfluoroarylation Using Sensitive Boronic Acids. *ACS Catal.* **2018**, *8*, 2989−2994. (d) Chen, L.; Sanchez, D. R.; Zhang, B.; Carrow, B. P. Cationic" Suzuki-Miyaura Coupling with Acutely Base-Sensitive Boronic Acids. *J. Am. Chem. Soc.* **2017**, *139*, 12418−12421.
(27) King, R. B.; Cloyd, J. C., Jr.; Reimann, R. H. Poly(tertiary phosphines and arsines). XIII. Some neopentyl poly(tertiary phosphines). *J. Org. Chem.* **1976**, *41*, 972−977.
(28) Li, H.; Grasa, G. A.; Colacot, T. J. A Highly Efficient, Practical, and General Route for the Synthesis of $(R_3P)_2Pd(0)$: Structural Evidence on the Reduction Mechanism of Pd(II) to Pd(0). *Org. Lett.* **2010**, *12*, 3332−3335.
(29) Pan, Y.; Young, G. B. Syntheses and spectroscopic characteristics of dialkylpalladium(II) complexes; $PdR_2(cod)$ as precursors for derivatives with N- or P-donor ligands. *J. Organomet. Chem.* **1999**, *577*, 257−264.
(30) *Saint Plus*, 8.34A; Bruker AXS Inc.: Madison, WI, 2007.
(31) (a) Sheldrick, G. M. *SHELXTL*, v. 2008; Göttingen University: Göttingen, Germany, 2008. (b) Sheldrick, G. M. A short history of SHELX. *Acta Crystallogr., Sect. A: Found. Crystallogr.* **2008**, *A64*, 112−122.
(32) Sheldrick, G. M. *SHELXL*, 2014/7; Göttingen University: Göttingen, Germany, 2014.
(33) Hübschle, C. B.; Sheldrick, G. M.; Dittrich, B. ShelXle: a Qt graphical user interface for SHELXL. *J. Appl. Crystallogr.* **2011**, *44*, 1281−1284.
(34) *CrysAlis Pro Software System*, V1.171.40.53; Rigaku Oxford Diffraction, 2019.
(35) Sheldrick, G. M. SHELXT - Integrated space-group and crystal-structure determination. *Acta Crystallogr., Sect. A: Found. Adv.* **2015**, *71*, 3−8.
(36) Sheldrick, G. M. Crystal structure refinement with ShelXL. *Acta Crystallogr., Sect. C: Struct. Chem.* **2015**, *71*, 3−8.
(37) Dolomanov, O. V.; Bourhis, L. J.; Gildea, R. J.; Howard, J. A. K.; Puschmann, H. OLEX2: a complete structure solution, refinement and analysis program. *J. Appl. Crystallogr.* **2009**, *42*, 339−341.
(38) Zhao, Y.; Truhlar, D. G. The M06 suite of density functionals for main group thermochemistry, thermochemical kinetics, noncovalent interactions, excited states, and transition elements: two new functionals and systematic testing of four M06-class functionals and 12 other functionals. *Theor. Chem. Acc.* **2008**, *120*, 215−241.
(39) Chai, J.-D.; Head-Gordon, M. Long-range corrected hybrid density functionals with damped atom-atom dispersion corrections. *Phys. Chem. Chem. Phys.* **2008**, *10*, 6615−6620.
(40) Frisch, M. J.; Trucks, G. W.; Schlegel, H. B.; Scuseria, G. E.; Robb, M. A.; Cheeseman, J. R.; Scalmani, G.; Barone, V.; Mennucci, B.; Petersson, G. A.; Nakatsuji, H.; Caricato, M.; Li, X.; Hratchian, H. P.; Izmaylov, A. F.; Bloino, J.; Zheng, G.; Sonnenberg, J. L.; Hada, M.; Ehara, M.; Toyota, K.; Fukuda, R.; Hasegawa, J.; Ishida, M.; Nakajima, T.; Honda, Y.; Kitao, O.; Nakai, H.; Vreven, T.; Montgomery, J. A., Jr.; Peralta, J. E.; Ogliaro, F.; Bearpark, M.; Heyd, J. J.; Brothers, E.; Kudin, K. N.; Staroverov, V. N.; Kobayashi, R.; Normand, J.; Raghavachari, K.; Rendell, A.; Burant, J. C.; Iyengar, S. S.; Tomasi, J.; Cossi, M.; Rega, N.; Millam, J. M.; Klene, M.; Knox, J. E.; Cross, J. B.; Bakken, V.; Adamo, C.; Jaramillo, J.; Gomperts, R.; Stratmann, R. E.; Yazyev, O.; Austin, A. J.; Cammi, R.; Pomelli, C.; Ochterski, J. W.; Martin, R. L.; Morokuma, K.; Zakrzewski, V. G.; Voth, G. A.; Salvador, P.; Dannenberg, J. J.; Dapprich, S.; Daniels, A. D.; Farkas, Ö.; Foresman, J. B.; Ortiz, J. V.; Cioslowski, J.; Fox, D. J. *Gaussian 09*, Revision B.1, Gaussian, Inc: Wallingford, CT, 2009.
(41) Tomasi, J.; Mennucci, B.; Cammi, R. Quantum mechanical continuum solvation models. *Chem. Rev.* **2005**, *105*, 2999−3093.
(42) Klamt, A.; Schüürmann, G. COSMO: A New Approach to Dielectric Screening in Solvents with Explicit Expressions for the Screening Energy and its Gradient. *J. Chem. Soc., Perkin Trans. 2* **1993**, *2*, 799−805.
(43) Frisch, M. J.; Trucks, G. W.; Schlegel, H. B.; Scuseria, G. E.; Robb, M. A.; Cheeseman, J. R.; Montgomery, J. A., Jr.; Vreven, T.; Kudin, K. N.; Burant, J. C.; Millam, J. M.; Iyengar, S. S.; Tomasi, J.; Barone, V.; Mennucci, B.; Cossi, M.; Scalmani, G.; Rega, N.; Petersson, G. A.; Nakatsuji, H.; Hada, M.; Ehara, M.; Toyota, K.; Fukuda, R.; Hasegawa, J.; Ishida, M.; Nakajima, T.; Honda, Y.; Kitao, O.; Nakai, H.; Klene, M.; Li, X.; Knox, J. E.; Hratchian, H. P.; Cross, J. B.; Adamo, C.; Jaramillo, J.; Gomperts, R.; Stratmann, R. E.; Yazyev, O.; Austin, A. J.; Cammi, R.; Pomelli, C.; Ochterski, J. W.; Ayala, P. Y.; Morokuma, K.; Voth, G. A.; Salvador, P.; Dannenberg, J. J.; Zakrzewski, V. G.; Dapprich, S.; Daniels, A. D.; Strain, M. C.; Farkas, O.; Malick, D. K.; Rabuck, A. D.; Raghavachari, K.; Foresman, J. B.; Ortiz, J. V.; Cui, Q.; Baboul, A. G.; Clifford, S.; Cioslowski, J.; Stefanov, B. B.; Liu, G.; Liashenko, A.; Piskorz, P.; Komaromi, I.; Martin, R. L.; Fox, D. J.; Keith, T.; Al-Laham, M. A.; Peng, C. Y.; Nanayakkara, A.; Challacombe, M.; Gill, P. M. W.; Johnson, B.; Chen, W.; Wong, M. W.; Gonzalez, C.; Pople, J. A. *Gaussian 03*, Revision E.01; Gaussian Inc: Wallingford, CT, 2004.
(44) Grimme, S.; Ehrlich, S.; Goerigk, L. Effect of the Damping Function in Dispersion Corrected Density Functional Theory. *J. Comput. Chem.* **2011**, *32*, 1456−1465.
(45) Becke, A. D. Density-functional thermochemistry. V. Systematic optimization of exchange-correlation functionals. *J. Chem. Phys.* **1997**, *107*, 8554−8560.
(46) Dunning, T. H., Jr. Gaussian basis sets for use in correlated molecular calculations. I. The atoms boron through neon and hydrogen. *J. Chem. Phys.* **1989**, *90*, 1007−1024.
(47) Kendall, R. A.; Dunning, T. H., Jr.; Harrison, R. J. Electron affinities of the first-row atoms revisited. Systematic basis sets and wave functions. *J. Chem. Phys.* **1992**, *96*, 6796−6806.
(48) Peterson, K. A. Systematically convergent basis sets with relativistic pseudopotentials. I. Correlation consistent basis sets for the post-d group 13−15 elements. *J. Chem. Phys.* **2003**, *119*, 11099−11112.
(49) Peterson, K. A.; Figgen, D.; Goll, E.; Stoll, H.; Dolg, M. Systematically convergent basis sets with relativistic pseudopotentials. II. Small-core pseudopotentials and correlation consistent basis sets for the post-d group 16−18 elements. *J. Chem. Phys.* **2003**, *119*, 11113−11123.
(50) Frisch, M. J.; Trucks, G. W.; Schlegel, H. B.; Scuseria, G. E.; Robb, M. A.; Cheeseman, J. R.; Scalmani, G.; Barone, V.; Petersson, G. A.; Nakatsuji, H.; Li, X.; Caricato, M.; Marenich, A. V.; Bloino, J.;

DOI: 10.1021/acs.inorgchem.9b02164
Inorg. Chem. 2019, 58, 13299−13313

Janesko, B. G.; Gomperts, R.; Mennucci, B.; Hratchian, H. P.; Ortiz, J. V.; Izmaylov, A. F.; Sonnenberg, J. L.; Williams-Young, D.; Ding, F.; Lipparini, F.; Egidi, F.; Goings, J.; Peng, B.; Petrone, A.; Henderson, T.; Ranasinghe, D.; Zakrzewski, V. G.; Gao, J.; Rega, N.; Zheng, G.; Liang, W.; Hada, M.; Ehara, M.; Toyota, K.; Fukuda, R.; Hasegawa, J.; Ishida, M.; Nakajima, T.; Honda, Y.; Kitao, O.; Nakai, H.; Vreven, T.; Throssell, K.; Montgomery, J. A., Jr.; Peralta, J. E.; Ogliaro, F.; Bearpark, M. J.; Heyd, J. J.; Brothers, E. N.; Kudin, K. N.; Staroverov, V. N.; Keith, T. A.; Kobayashi, R.; Normand, J.; Raghavachari, K.; Rendell, A. P.; Burant, J. C.; Iyengar, S. S.; Tomasi, J.; Cossi, M.; Millam, J. M.; Klene, M.; Adamo, C.; Cammi, R.; Ochterski, J. W.; Martin, R. L.; Morokuma, K.; Farkas, O.; Foresman, J. B.; Fox, D. J. *Gaussian 16*, revision A.03; Gaussian, Inc: Wllingford, CT, 2016.

DOI: 10.1021/acs.inorgchem.9b02164
Inorg. Chem. 2019, 58, 13299−13313